

ANALYSIS OF AN EXPOSED PORTION OF THE BADWATER TURTLEBACK  
SHEAR-ZONE, DEATH VALLEY, CALIFORNIA, USA

by

COREY BRANTLEY JARRETT

A THESIS

Presented to the Department of Earth Sciences  
and the Graduate School of the University of Oregon  
in partial fulfillment of the requirements  
for the degree of  
Master of Science

December 2017

THESIS APPROVAL PAGE

Student: Corey Brantley Jarrett

Title: Analysis of an Exposed Portion of the Badwater Turtleback Shear-zone, Death Valley, California, USA

This thesis has been accepted and approved in partial fulfillment of the requirements for the Master of Science degree in the Department of Earth Sciences by:

Marli Miller	Chairperson
Ray Weldon	Member
Mark Reed	Member

and

Sara D. Hodges	Interim Vice Provost and Dean of the Graduate School
----------------	--

Original approval signatures are on file with the University of Oregon Graduate School.

Degree awarded December 2017

© 2017 Corey Brantley Jarrett  
This work is licensed under a Creative Commons  
**Attribution-NonCommercial-NoDerivs (United States) License**



## THESIS ABSTRACT

Corey Brantley Jarrett

Master of Science

Department of Earth Sciences

December 2017

Title: Analysis of an Exposed Portion of the Badwater Turtleback Shear-zone, Death Valley, California, USA

The exposed shear zone within the footwall of the Badwater turtleback presents an excellent opportunity to explore the brittle-ductile transition. Within this shear zone, a variety of lithologies preserve the last stages of crystal-plastic deformation concurrent with exhumation of the turtleback. The included field study captures a snapshot of each lithologic element during the last stages of ductile deformation.

The exposed shear zone's journey through the brittle-ductile transition is analyzed using the deformation mechanisms of calcite and quartz. A history of strain partitioning is constructed through comparison of the strain and temperature environments needed to facilitate each mechanism of crystal-plastic deformation. As the shear zone cooled, strain was partitioned from quartz-rich mylonitic gneiss to the calcite-dominated marbles and mylonites. Correlation of deformation temperatures with previous studies further constrains the timing of the last stage of ductile deformation to between 13 and 6 Ma.

## CURRICULUM VITAE

NAME OF AUTHOR: Corey Brantley Jarrett

### GRADUATE AND UNDERGRADUATE SCHOOLS ATTENDED:

University of Oregon, Eugene  
University of Colorado, Boulder  
Colorado School of Mines, Golden

### DEGREES AWARDED:

Master of Science, Geology, 2017, University of Oregon  
Bachelor of Arts, Geology, 2015, University of Colorado

### AREAS OF SPECIAL INTEREST:

Structural Geology  
Education and Science Outreach

### PROFESSIONAL EXPERIENCE:

Graduate Teaching Fellow, University of Oregon, 2015-2017  
Undergraduate Research Assistant, University of Colorado, 2014-2015

### GRANTS, AWARDS, AND HONORS:

Graduate Teaching Fellowship, 2015 - 2017  
UO Department of Earth Sciences, Johnston Scholarship, 2016  
Geologic Society of America Student Travel Grant, 2016  
UO Department of Earth Sciences, Weiser Scholarship, 2017

## ACKNOWLEDGMENTS

I would like to thank my thesis advisor and mentor Marli Miller, without whom this project would not have been possible. Her academic, geologic, emotional and financial support has contributed much not only to my development as a geoscientist, but also to a better understanding of myself. I hope that her dedication to education and outreach continues to inspire many students.

I thank Ray Weldon and Mark Reed for their support and feedback as members of my thesis committee. Their contributions along with the supportive academic atmosphere of the Department of Earth Sciences helped inspire and expand my work. I would also like to thank Nancy Price, whose insights on microstructures and project design helped greatly in understanding the processes at work in the Badwater turtleback.

Additionally, I extend special thanks to the University of Oregon graduate student community which has always worked to be inclusive and supportive. There are too many to name here, but their collective work, positive attitudes, and emotional support inspired me to push my own boundaries in both science and in giving back to the community.

## TABLE OF CONTENTS

Chapter	Page
I. INTRODUCTION .....	01
II. BACKGROUND INFORMATION.....	04
Geology of the Black Mountains .....	04
Review of Work in Death Valley Relevant to the Badwater Turtleback.....	08
Review of Work on Calcite Deformation and Strain Analysis.....	12
III. SITE STUDY .....	15
Lithologic Elements .....	20
Gneiss .....	20
Marble Elements .....	22
Marble 1 .....	22
Marble 2A .....	26
Marble 2B .....	27
Pegmatite.....	29
Diabase.....	31
Structures .....	32
IV. METHODS .....	34
Field Work .....	34
Thin Sections .....	36
Strain Analysis .....	37

Chapter	Page
V. RESULTS .....	40
Strain Analysis .....	40
Grain Size Distribution .....	43
Foliation and Lineation Orientations .....	44
VI. DISCUSSION AND CONCLUSIONS .....	45
Deformation Mechanisms .....	45
Quartz Deformation .....	46
Calcite Deformation .....	48
Strain Partitioning .....	52
Conclusions .....	54
APPENDICES .....	56
A. FOLIATIONS AND LINEATIONS .....	56
B. SAMPLES .....	57
C. THIN SECTIONS .....	58
REFERENCES CITED .....	60
SUPPLEMENTAL FILES	
IMAGE: FIELD MAP OF CANYON 1	
IMAGE: FIELD MAP OF CANYON 2	
PDF: FIELD NOTES 9/20/15-4/20/16	
PDF: FIELD NOTES 12/13/16-12/20/16	



## LIST OF FIGURES

Figure	Page
1. Map of Badwater turtleback extent and photographs .....	05
2. Map of the exposed shear zone in two canyons.....	16
3. Shear zone features: Corrugations and foliations .....	18
4. Schematic cross section of the Badwater turtleback exposed shear zone.....	19
5. Gneiss outcrop and photomicrographs.....	21
6. Marble 1 outcrop and photomicrograph .....	23
7. Marble 2A outcrop and photomicrograph.....	26
8. Marble 2B outcrop and photomicrograph.....	28
9. Diabase and pegmatite features .....	30
10. Faults and breccia .....	32
11. Fry plots for Marble 1 and Marble 2A.....	41
12. Calcite grain size distributions.....	42
13. Foliation and Lineation Stereonets .....	43
14. Types of calcite twins from Burkhard (1992).....	49
15. Shear models.....	51

# CHAPTER I

## INTRODUCTION

The brittle-ductile transition defines the boundary zone where deformation in rocks switches from breaking and cracking to stretching, and folding. While the brittle-ductile transition is generally defined as occurring at 300-400° C or at an equivalent depth of 13-17 km for quartzo-feldspathic rocks, there is much more going on at this transition than just a change in numbers. At the micro-scale, individual grains change size and orientation, switching from cataclastic flow to crystal plastic deformation, and creating textures like mylonites, mélanges, and mica fish in the process. The implications for this transition go beyond the visual differences of how rocks deform. The brittle-ductile transition is one of the fundamental boundaries within the Earth's interior important to understanding thick-crust tectonic interactions, and how earthquakes are nucleated within the crust. The Badwater turtleback, and the exposed portion of the shear zone on its slopes, offers a window into this state of transition.

Transition from ductile to brittle is controlled by two factors: temperature, strain rate. As temperature decreases in deforming rocks, the capacity for ductile deformation drops until the rock snaps and cracks. Similarly, if the strain builds too quickly for ductile mechanisms, the rock will also break. The footwall shear zone exposure at Badwater turtleback features both brittle and ductile structures, a signature of the passage through the ductile-brittle transition. This makes the Badwater turtleback an excellent place to study just how this process unfolds. Different lithologies within the shear zone

experience totally different histories of deformation under the same temperatures and strain rates, creating a readily accessible laboratory within which to make comparisons.

For nearly a century, geologists have mapped and studied the Black Mountains of Death Valley to discern their origin and history. Previous workers recognized that the Badwater turtleback contains a high-strain, ductile shear zone, but my work goes beyond that to look at the shear zone in minute detail, characterizing individual lithologies and how strain is accommodated in each of them. Each unit tells a story of changing deformation styles as the temperature decreased, until only brittle deformation was possible. Understanding this progression is necessary to compiling a history of the shear zone.

My study details the progression of strain localization in the exposed shear zone. This includes evidence of cooling over the history of deformation, and the partitioning of strain across the exposed shear zone from contrasts in rheology. I demonstrate that the temperature decreased over time in the exposed shear zone. Also, I attempt to correlate my findings with the interpretation put forth by previous workers that turtleback was deforming while being uplifted and denuded.

This manuscript includes a review of pertinent concepts and related literature, field observations of rocks and structures from my field work, laboratory observations using a variety of methods, and my interpretations of these observations. Additionally, my outreach and the resultant feedback from fellow researchers I received at two public presentations at the Geological Society of America Annual Meeting, in 2016 and 2017, played an important role in my interpretations.

This thesis is split into six chapters, including the introduction. Following the introduction is a review of the geologic background and previous work related to my study area. I describe the field site in detail and my methods for collecting and analyzing data. The thesis ends with a summary of the results of my analysis, and my interpretations of the work as a whole. This includes a summary of conclusions and discussion of future work that could utilize my results and interpretations to further the understanding of the brittle-ductile transition.

## **CHAPTER II**

### **BACKGROUND INFORMATION**

I begin with an overview of the Black Mountains, which includes the focus of my work, namely the Badwater turtleback, the origin of the Black Mountains, and the events and lithologies that define them. Following that I briefly review the work done by previous researchers in the Black Mountains, and finish this background survey with an overview of work on calcite microstructures and how strain analysis has been applied to analyze calcite deformation.

#### **Geology of the Black Mountains**

The Badwater turtleback (Figure 1A), a doubly-plunging antiform, lies within the central portion of the Black Mountains, which form the eastern wall of the southern end of Death Valley. The Black Mountains themselves form a part of the Amargosa Range, which runs the entire length of the eastern portion of Death Valley National Park (DVNP), California. Together with the Panamint Range to the west, these two mountain ranges define the boundaries of Death Valley. All of these features are found within the arid and low-lying Mojave Desert of southeastern California. These conditions lend themselves to creating excellent rock exposures, free of loose sediment, soil and plant cover.

The geologic history of the Badwater turtleback cannot be separated from the history of the Black Mountains. Although small in area, the Badwater turtleback displays many features typical of a Cordilleran Metamorphic Core Complex (Armstrong, 1982).

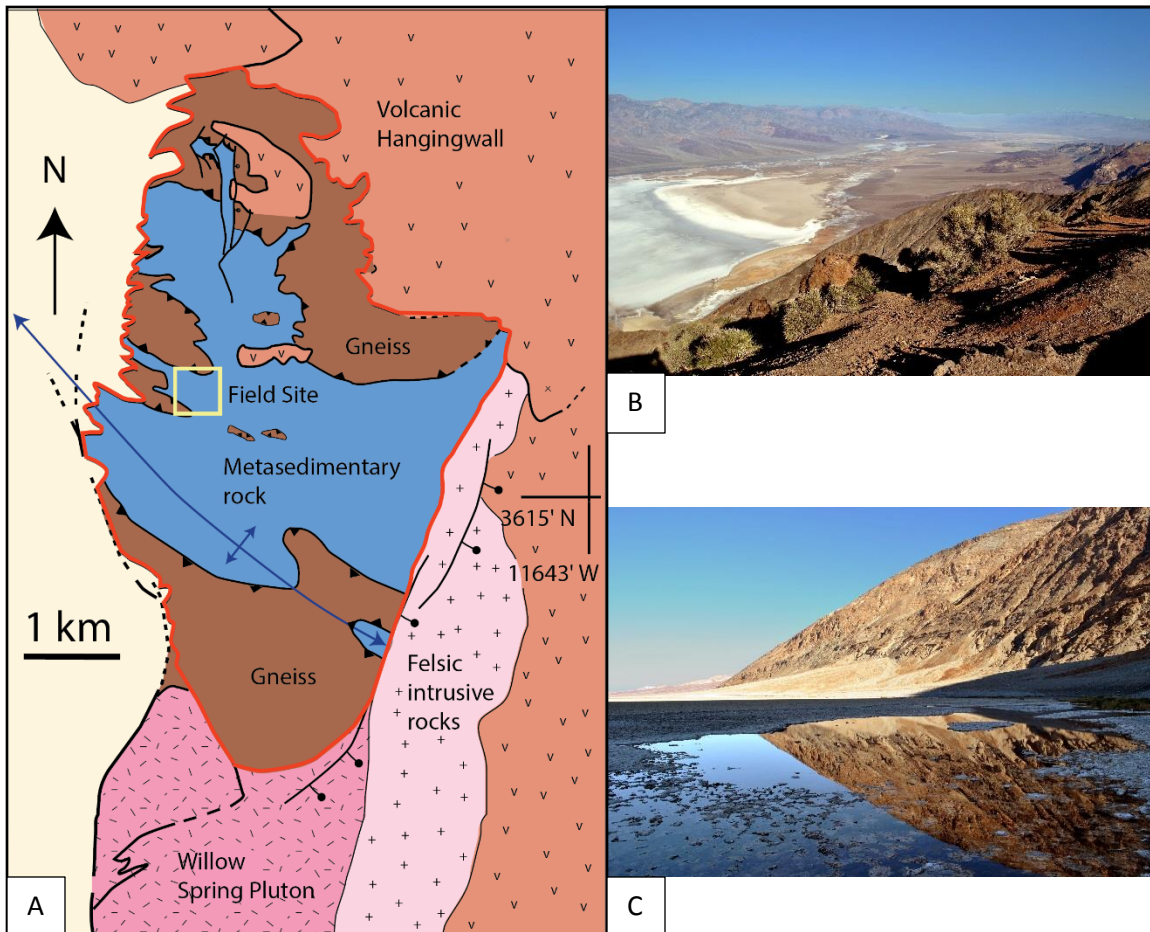


Figure 1. A. Map of Badwater Turtleback, extent shown in red. Adapted from Miller and Pavlis, 2015. Area of investigation is shown in the yellow box. B. Death Valley from Dante's View, Badwater Turtleback can be seen in the foreground. C. Badwater turtleback from the valley floor, at Badwater Spring.

The defining features include a ductilely deformed basement footwall and highly faulted upper crustal hanging wall separated by a brittle, extensional fault zone (Davis, 1980; Armstrong, 1982; Davis and Lister, 1988). In the Badwater turtleback, the deformed core is made up of basement gneiss, calc-mylonitic mélanges, and crystalline marble (Miller, 2005).

The Black Mountains contain a basement of Precambrian gneiss overlain by younger metasedimentary rock. As the Black Mountains developed, these units were

intruded by early Paleogene diabase and mid-to-late Neogene pegmatite, and then capped by late-Neogene volcanic rock (Holm 1992, Knott et al., 2005; Miller and Pavlis, 2005). The region has experienced significant deformation from compressional and extensional tectonic settings, and today sits in at the northern end of the Eastern California Shear Zone, which runs along the California-Nevada border into Arizona (Faulds et al., 2005).

The basement gneiss is the oldest rock in the core of the Black Mountains, and is derived from Proterozoic rocks that underwent regional metamorphism in the late Paleoproterozoic (Miller and Wright, 2002). Following the formation of the gneiss basement, Proterozoic biogenic- and clastic-sedimentary rock of the Parhump Group were deposited in a basin, described by Wright and Troxel as a failed rift (1984). The Proterozoic sediment was metamorphosed into the marbles found in the Black Mountains today (Wright et al., 1976). The marbles in the Badwater turtleback footwall may either be equivalent to the Crystal Spring Formation or the Noonday Dolomite (Wright et al. 1976; Creverling, 2016). However, the exact correlation of these formations with the marbles is still uncertain.

The crystalline basement was at one point overlain by late-Proterozoic and Paleozoic rocks of western North America's passive margin (Creverling, 2016). Most of these rocks were later removed by uplift and unroofing during the extension of the Basin and Range province and are mostly missing in the modern Black Mountains. However, scattered exposures do exist, which helps support this history (Stewart, 1983; Wernicke, 1989; Keener, 1993; Miller and Prave, 2002).

During the late Mesozoic and early Paleogene, the gneiss, marble and overlying sediments were compressed during crustal shortening, possibly coinciding with the Laramide orogeny (Schmandt and Humphreys, 2011; Flesch and Bendrick, 2012; Wernicke, 2008). This shortening resulted in multiple north-striking thrust faults in the roots of the Black Mountains. These thrusts placed basement rocks over Proterozoic metasedimentary rocks, with gneiss and marble repeated in the stratigraphy of the turtlebacks as a result (Miller, 2003). Pegmatite intrusions accompanied this deformation, uplifting the terrain (Miller and Friedman, 1999).

By the late Paleogene, the tectonic regime shifted from compression to extension (Dokka and Ross, 1995; Wernicke et al., 2008). It was during this time that the extensional faults that define the surface of the turtlebacks took shape. The exact nature of these extensional faults is still debatable. An interpretation is that old thrust faults were reactivated as extensional faults, pulling apart the basement rock of the Black Mountains (Miller, 2003; Miller and Pavlis, 2005). This early extension was still deep underground, with pegmatite emplacement and cooling beginning around 20 km depth (Whitney et al., 1993). The initiation of extension while the basement was still at this depth is key to the formation of the rocks seen on the turtleback today.

Crustal extension and denudation of Black Mountain turtlebacks started between 16-18 Ma (Holm et al., 1994; Miller and Friedman, 1999). The pulling apart of the valley, with strike-slip faults to the north and south, began in the mid-to-late Neogene (Burchfiel and Stewart, 1966; Serpa and Pavlis, 1996; Miller and Prave, 2002; Miller and Pavlis, 2005). During that time, the turtleback faults were reactivated and the turtleback surfaces were subsequently exhumed. Igneous intrusions came after the late Neogene



episode of extension, with basalt dikes and sills cutting the Black Mountains around 6 Ma (Holm et al. 1992). The window between 18 and 6 Ma is of particular interest because the transition from ductile to brittle deformation in the footwall of the turtleback could only have occurred during this time (Miller and Friedman, 1999).

Today, there is still movement along the faults that define the front of the Black Mountains, as seen from the many fault scarps present in alluvial fans (Burchfiel et al., 1987). Most of the turtlebacks are currently well exposed, with only very limited sedimentary rock cover. Modern alluvial fan sediments cover some of the surface with thin layers of cobble-sized scree or sand, but otherwise the current turtleback surfaces are exposed to weathering. However, given the dry climate, reworking of the landscape has been slow and deeper rocks in the core of the turtleback remain out of reach for observation.

### **Review of work in Death Valley relevant to the Badwater turtleback**

Understanding the geologic history and findings from previous work supports the significance and interpretations of my investigation. Studying the brittle-ductile transition in the Badwater turtleback is only possible through discoveries which lead to the current interpretation of the Black Mountain turtlebacks as extensional features with highly strained footwalls.

Geologic and structural investigations of the Black Mountains stretch back to the early twentieth century. The turtlebacks of the Black Mountains were first named by Curry (1938) for their resemblance to the shell of the eponymous reptile. There are three turtlebacks along the front of the Black Mountains. From south to north they are the

Mormon Point, Copper Canyon, and Badwater turtlebacks (Miller and Wright, 2002).

The turtlebacks and the surrounding desert have been the focus of many research projects.

Early work focused on mapping and describing the rock units and structures of the area, laying the foundation for later research. This early period covers the first half of the twentieth century and includes work by Curry (1938, 1954), Noble (1934, 1941), Sears (1953), and Drewes (1959). Drewes's work in 1959 was particularly focused on the turtleback surfaces and normal faults, where he concluded that the turtleback faults were extensional and the result of gravity-driven forces. Curry had previously interpreted the turtleback faults as thrust faults, but neither his nor Drewes's interpretations entirely matches with the present interpretation of a deep-rooted extensional fault.

In the second half of the twentieth century, investigations focused more on connecting the geology of Death Valley with tectonics and the surrounding region. In 1954 Noble and Wright produced an overview of the geology of the Mojave Desert, including Death Valley, recognizing that Death Valley did indeed fit within a larger picture of the region. In 1966, Hill and Troxel produced a study on the tectonics of the Death Valley region, noting that both compression and extension played a role in the extant geology. In 1966 as well, Burchfiel and Stewart recognized that there could be a connection between the strike-slip faults that bounded central Death Valley and the extensional faults along the front of the Black Mountains. In the same year, Hamilton and Myers produced an overview of Cenozoic tectonics in the western United States, placing the work of the previous two reports in a broader context. This would be

important for later work investigating the regional stresses that influenced the deformation of the turtlebacks.

Building upon the 1966 reports, Wright (1976) argued that the normal faults of late-Cenozoic age in the Basin and Range province, as occur at the front of the Black Mountains, were a first order result of strike-slip faults. He argued that these faults were driven by stresses of the extension of the southern Basin and Range province, with the minimum, principle stress parallel to a west-northwest trend. This is an important distinction of the strain environment to keep in mind for my study. Together, Wright and Troxel would become some of the most prolific workers in Death Valley geology at that time.

Their most significant contribution to the understanding of Badwater turtleback was Wright, Otton and Troxel's 1974 paper, "Turtleback surfaces of Death Valley viewed as phenomena of extensional tectonics." This paper was the first to depart from Drewes interpretation of the turtleback faults as gravity driven. Instead, the authors proposed that the turtlebacks were deep-rooted normal faults with tectonic origins. Without this interpretation it would be difficult to argue that the footwall shear zone of the Badwater turtleback records a history of cooling and exhumation related to the fault above it.

Explaining how these deep-rooted faults developed was difficult. Anderson's work in 1971 on thin-skinned tectonics in the basin and range attempted to describe the rotated fault blocks as the result of igneous intrusions. In 1983 Stewart suggested that large detachment faults may better describe the pull-apart formation of Death Valley. He

proposed a structural connection between the modern Panamint Range, to the west, and the Black Mountains, building on work by Hunt and Mabey (1966). Later studies by Butler et al. (1988) and Hamilton (1988) both recognized these detachments, but Butler argued that the offset seen in the southern Death Valley was not great enough to support Stewart's interpretation. The topic of the detachment and its role and in the connection between the Black Mountains and the Panamint Range is still debated today. However, it is important to my own interpretations that the surface of the Badwater turtleback is considered a detachment fault.

The stratigraphy of the region is important for connecting marbles in the turtleback to a protolith in the region. Hunt and Mabey produced a comprehensive study of Death Valley structures and stratigraphy in 1966 for the US Department of the Interior Geological Survey. Notable was their early recognition that part of Death Valley may feature a detachment fault, although its significance was beyond the scope of their investigation. Their stratigraphic work is useful to interpreting the origin of the marble in the footwall shear zone at Badwater. A more modern stratigraphic study that can be applied to the turtlebacks was done by Creverling et al. (2016), whose investigation of the Noonday Formation produced a detailed stratigraphic column and a facies model that supports a rift-basin for the deposition of the Proterozoic carbonate rock.

Detailed studies of the turtlebacks and their shear zones are limited to recent literature. Miller has produced a great deal of work related to Death Valley, the turtlebacks, and describing the footwall shear zone. Her investigations in 1991 sought to resolve the problem of the Badwater turtleback surface being interpreted as a low-angle detachment fault. She argued that the fault had formed at a high angle and then was

rotated. This claim better supports the interpretation of Death Valley extension as advocated by Stewart (1983). This assertion was by Miller and Prave in 2002, where they found that the rolling-hinge model, like the model supported by Stewart and proposed in her 1991 paper, was less likely than deeply-rooted fault systems. In 1992, Miller first described the Badwater turtleback and the ductile deformation of the footwall in detail, arguing that the calcite marbles were the last to deform crystal-plastically, which is a starting point for my own investigation. Mancktelow and Pavlis also described folding in the basement of the turtlebacks in 1994, where they noted the corrugations seen in my own study. Miller's work in 2003 went on to describe the basement thrusts which place gneiss over marbles in the turtleback, which she concluded were related to thick-skin deformation around the time of the Laramide orogeny. All of these interpretations are important to understanding the context of the shear zone within my study.

Constraining the deformation on the turtleback is possible due to the work of Holm et al. (1992). They determined the constraints on the intrusions and unroofing of the Black Mountains, placing denudation around 13-6.8 Ma. Holm and Dokka (1993) further constrained the unroofing of the central Black Mountains, which includes the Badwater turtleback, to 8.5-6.0 Ma, for unroofing from temperatures of 300° C. These details are key to supporting the cooling history observed from calcite deformation in this report.

### **Review of work on Calcite Deformation and Strain Analysis**

For this study, calcite is the primary mineral used for strain analysis, although

quartz is also considered. Significant work on the modern, well developed understanding of calcite deformation took place in the 1970s, with a focus on the effects of water on calcite deformation and on using mechanical twinning as a strain gauge.

Rutter (1970, 1972, 1974) found that the presence of water weakens the rheologic strength of calcite, although the pore pressure of water has little effect on deformation mechanisms. Groshong (1972, 1974; et al. 1984) investigated the use of mechanical twinning in calcite as a gauge for strain. He found that calcite twins are best used for measuring relatively low-strain deformation, but the process is quite mathematically complex.

Calcite is notable for its ability to accommodate strain by crystal plasticity through ductile deformation even at relatively low temperatures for the Earth's interior. This feature is a useful tool for documenting the transition from ductile to brittle deformation, as other minerals, like quartz, stop deforming crystal-plastically at much higher temperatures. Mechanical twinning is the dominant expression of deformation in calcite at low temperatures and has been thoroughly characterized by Burkard in 1992. He defines calcite twins by width and shape, and provides constraints on the amount of strain and temperature ranges necessary for each. This classification system is vitally important to my interpretations of the cooling history of the Badwater turtleback shear zone.

While not specific to calcite, Fry developed the center-to-center strain analysis technique in 1979, also known as the Fry method. This method is graphical, utilizing a plot of the orientation and spacing between the center of objects to generate a finite strain

ellipse. While difficult to implement, the process is still quite time consuming.

Thankfully, future refinements by Mulchrone (2013) made the process semi-automated and more objective, reducing the time needed to produce a plot using the Fry method.

Strain analysis using center-to-center methods is not exclusive to calcite, but was developed and refined over the same period. Following Fry in 1979, Erslev developed the normalized Fry method (1988) and the enhanced normalized Fry method (Erslev et al. 1990), which both improved the objectivity of the Fry method.

Advancements in computer processing power made it possible to move the Fry method from a graphical method to a numerical one. Mulchrone's work in the early 2000s introduced Delaunay triangulation to the Fry method. This refined method looks at groups of nearest neighbors in addition to the normalized center-to-center distances to ensure an objective fit (Mulchrone, 2002; Meere and Mulchrone, 2003; Mulchrone et al., 2003). Further refinement and tuning of this method to optimize it for use with computers was done by Waldron and Wallace in 2007. In 2013, Mulchrone et al. developed and published a semi-automated form of the Delaunay triangulation Fry method in Wolfram Mathematica, greatly simplifying the process of generating Fry plots. This tool makes developing Fry plots for strain analysis more accessible and objective for researchers like myself.

## CHAPTER III

### SITE STUDY

My study site covers two canyons on the steep, northwestern slope of the Badwater turtleback. Each canyon runs approximately east-west through the study area. Boundaries of the study area coincide with places where the canyon changes its strike significantly or becomes impassible (Figure 2A, B). Spatially, the two canyons are separated by approximately 150 meters, with Canyon 1 being the southern-most of the two.

There is little variation in the exposed lithologies across this distance, so my model of the shear zone relies on a synthesis of observations from the two canyons. Each canyon exposes a cross section of the uppermost part of the footwall shear zone, approximately 100 meters long and 30 meters deep, as measured from the canyon rim. Outside the canyons, outcrops are present, but reveal only the top-most part of the shear zone. Surfaces outside the canyons are also partially obscured by talus.

Lithologies of the exposed portion of the shear zone are primarily Proterozoic metamorphic rocks. The crystalline basement rock consists of Proterozoic gneiss. Overlying the gneiss is a relatively thin skin of Proterozoic calc-mylonite mélanges and marbles. Also present are small fragments of pegmatite and 12 diabase dikes. None of the pegmatite in the shear zone was originally emplaced there, and only exists as fragments and boudins within other elements today. The age at which the pegmatite was originally emplaced is the 55 Ma (Miller and Friedman, 1999; Miller and Pavlis, 2005).



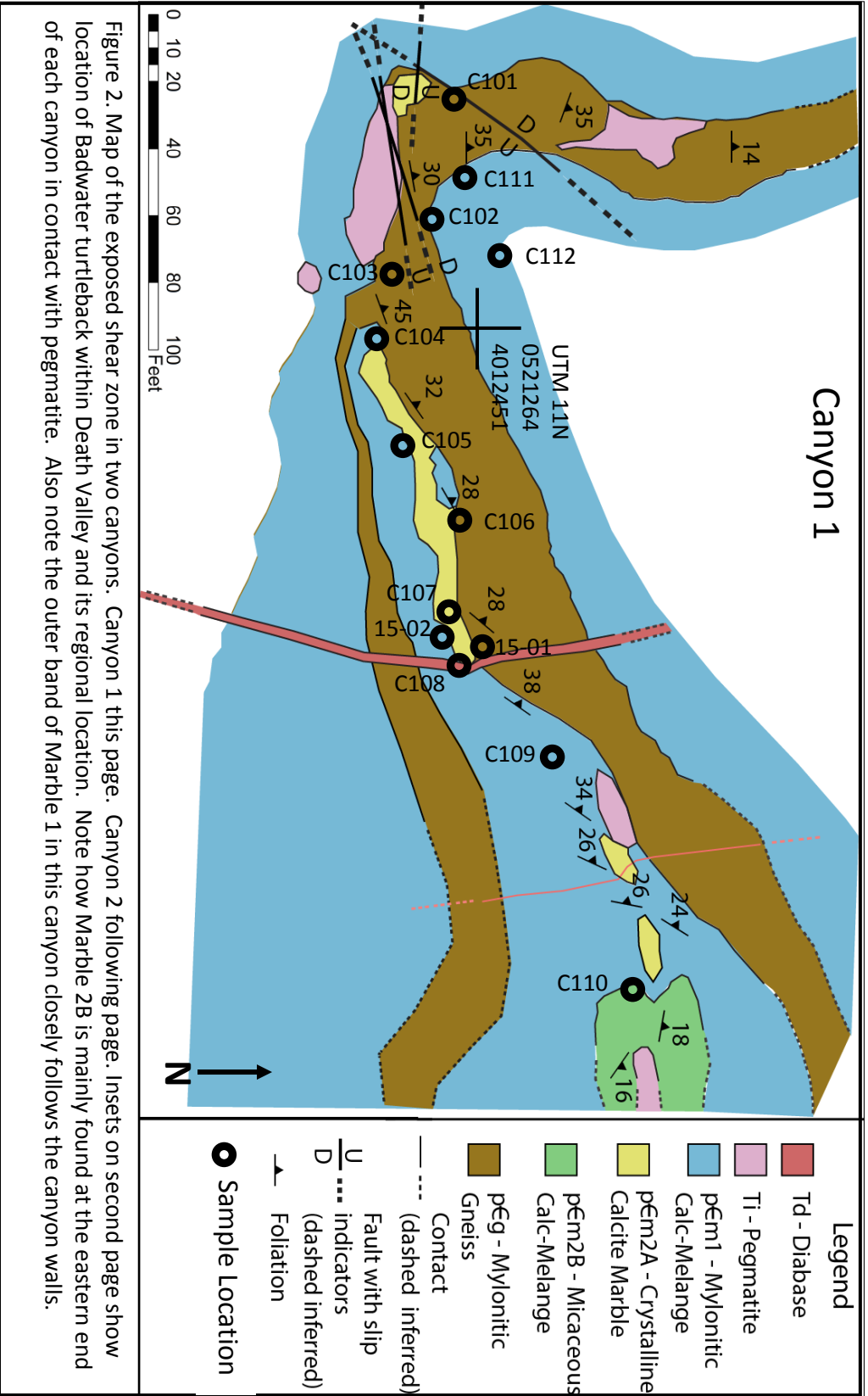


Figure 2. Map of the exposed shear zone in two canyons. Canyon 1 this page. Canyon 2 following page. Insets on second page show location of Badwater turtleback within Death Valley and its regional location. Note how Marble 2B is mainly found at the eastern end of each canyon in contact with pegmatite. Also note the outer band of Marble 1 in this canyon closely follows the canyon walls.

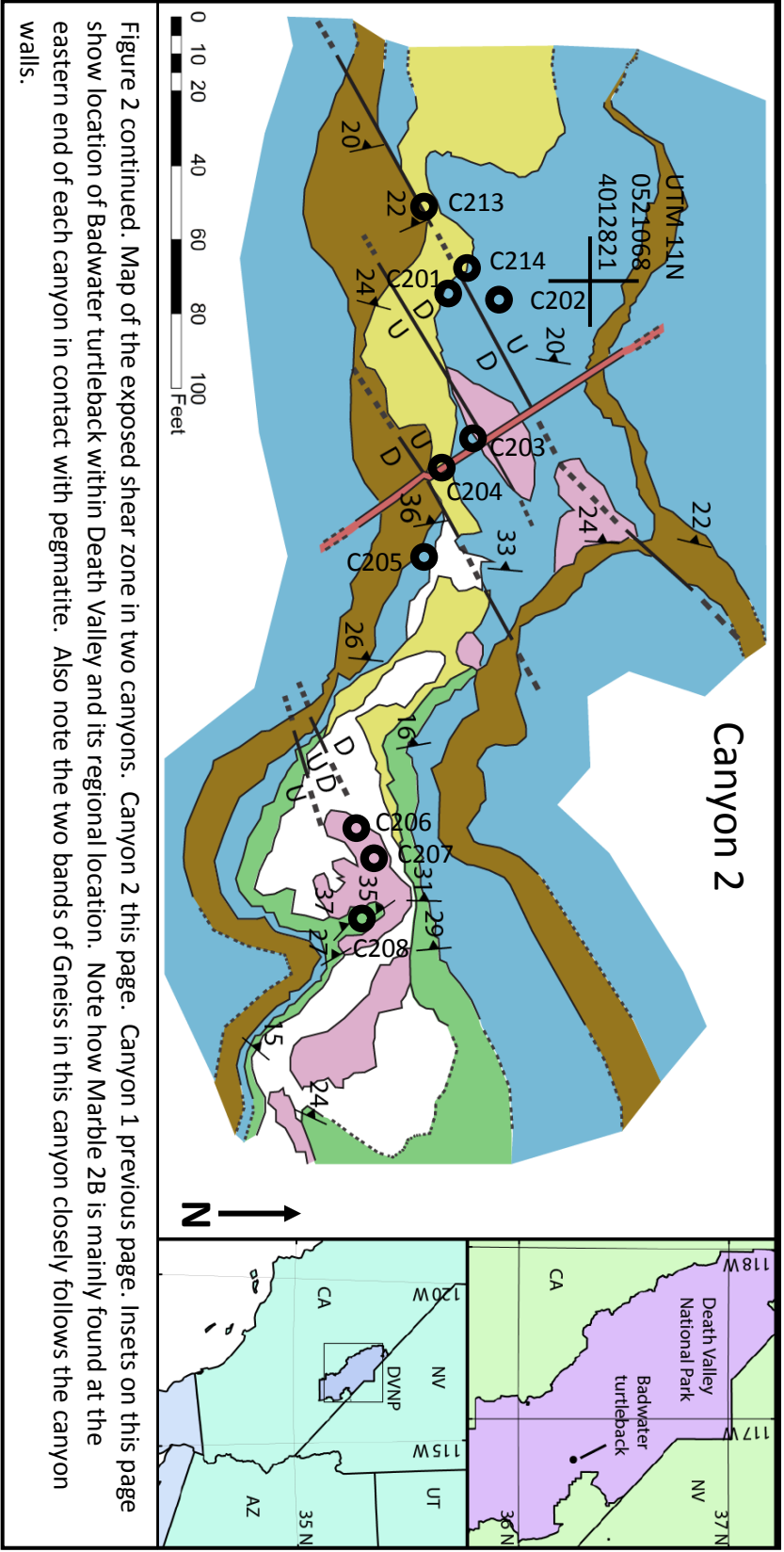


Figure 2 continued. Map of the exposed shear zone in two canyons. Canyon 2 this page. Canyon 1 previous page. Insets on this page show location of Badwater turtleback within Death Valley and its regional location. Note how Marble 2B is mainly found at the eastern end of each canyon in contact with pegmatite. Also note the two bands of Gneiss in this canyon closely follows the canyon walls.



Figure 3. Shear zone features: Corrugations and foliations. A. Corrugation or possibly a mullion between gneiss and Marble 1 surface. Gneiss sits above the line and Marble 1 is below. B. Foliation in Marble 1, note the mineral segregation that defines the foliation is defined by more calc or silica minerals.

The diabase is much younger, having intruded the country rock at approximately 6-8 Ma, and forms dikes in both canyons (Holm, 1992).

I classified the rocks into six elements: three marbles, gneiss, and the two igneous rocks. These elements are defined by their differences in lithology and structure. Some elements that share lithologies are further broken down by mineralogy and structure. I cover these elements in detail in the next section.

The exposed portion of the shear zone is planar, with some meso-scale corrugations. With one exception, the metamorphic elements have a penetrative foliation that parallels the plane of the shear zone (Figure 3B). Generally, the foliation strikes to the northeast and dips to the northwest to west. The hinge line of the corrugations parallels the dip direction of the foliation plane. The corrugations are on the scale of 15 to 20 meters in wavelength, with an amplitude of less than 3 meters (Figure 3A). They are better defined in the southern canyon than in the northern canyon. Similar corrugations have been observed at other locales in the turtlebacks (Mancktelow and Pavlis, 1994). In the northern canyon, foliations almost all dip gently to the northwest.

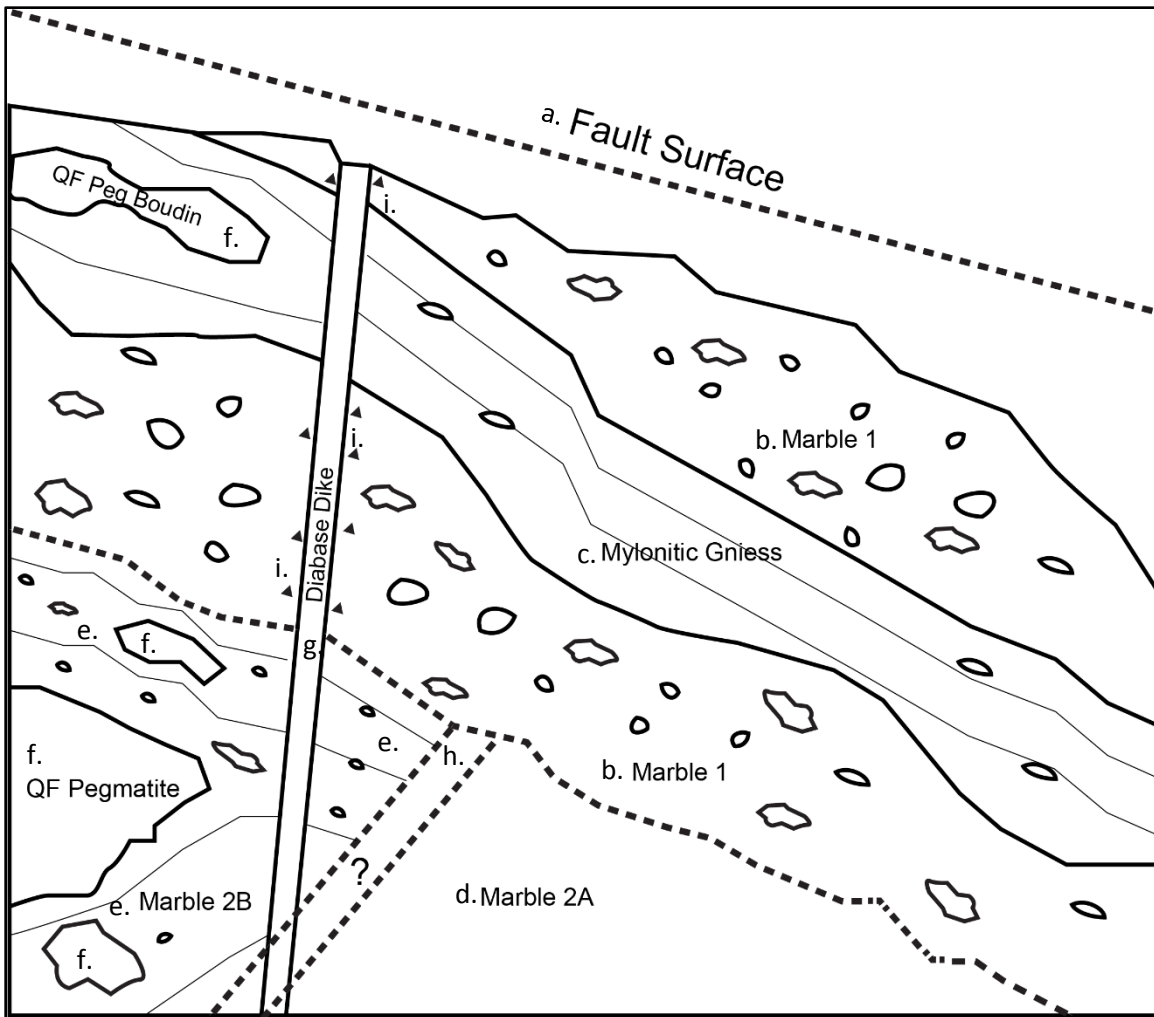


Figure 4. Schematic cross section of the Badwater turtleback exposed shear zone, illustrating the removed extensional fault surface at top a., and each of the lithologic elements and contacts. Marble 1 with fragments b., mylonitic gneiss c., Marble 2A d., Marble 2B e., pegmatite fragments f., diabase dike g., uncertain transition between Marbles 2A and 2B h., diabase fragments i. Dashed contacts are gradational, while solid contacts are sharp, thin lines indicate foliation.

The sole exception to this behavior is Marble 2B, which is in wide-spread contact with pegmatite fragments. I discuss the significance of this contact in the next section.

Structures that affect multiple elements, such as faults, are covered in more detail following the overview of lithologic elements.

## **Lithologic Elements**

I defined six elements of the shear zone based on lithology, mineralogy, and structure. Four are metamorphic and two are igneous. These elements display both brittle and ductile deformation confined to individual elements and in structures that crosscut all elements. The metamorphic units in structural order, starting at the top of the exposed portion of the shear zone, are Marble 1, the Gneiss, Marble 2A and Marble 2B (Figure 4). The igneous pegmatite occur as fragments in the mylonites. The mafic dike, simply crosscuts all the units present (Figure 4).

### *Gneiss*

The oldest unit in the shear zone consists of Proterozoic basement gneiss, initially mylonitized during the late Cretaceous to Early Paleogene compression (Miller and Pavlis, 2005). In the Badwater turtleback, and in the other turtlebacks of the Black Mountains, the exposed gneiss sits above Marble 1 because the gneiss was thrust over Marble 1, a contact described by Miller and Friedman as a basement involved thrust fault (1999). At the base of the turtleback, not far from where it meets the alluvial fan, the gneiss can be observed repeating in the stratigraphic sequence.

Within the gneiss, minerals are well segregated into light and dark bands with scattered porphyroclasts, no larger than 2 cm in diameter. The mineral banding defines a foliation plane that strikes northeast and dips to the northwest. The banding thickness ranges from less than a millimeter to 8mm. A penetrative lineation trends and plunges in the same orientation as the dip of the foliation. In the plane parallel to lineation, the porphyroclasts display weak strain shadows that indicate top to the northwest translation.



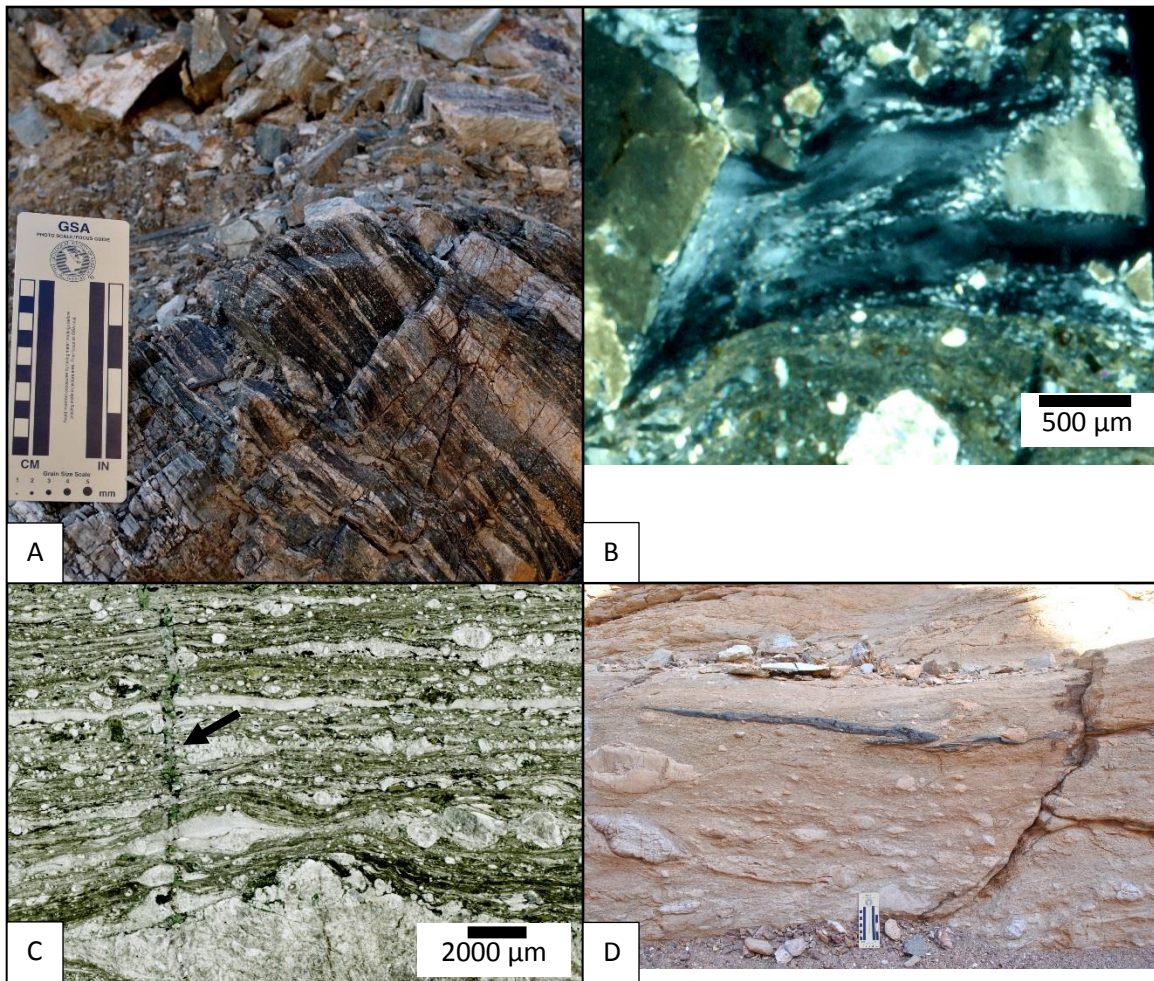


Figure 5. Gneiss outcrop and photomicrographs A. Outcrop of mylonitic gneiss B. Photomicrograph under cross-polarized light of crystal-plastic deformation in quartz. Note the speckled texture, this shows both sub-grain rotation and the undulose extinction in the quartz. C. Photomicrograph under plane-polarized light, showing chlorite vein (see arrow) and top-to-right shear sense. D. Pyritically folded gneiss fragment in Marble 2B resulting from the large difference in rheological strength between the silica rich gneiss and the calc rich marble.

Grain size throughout the gneiss is very small outside of porphyroclasts, typically on the order of 50 micrometers, down to around one micrometer in diameter in highly recrystallized areas (Figure 5B). The gneiss is dominated by quartz and feldspars, accompanied by chlorite, which is found throughout the gneiss, but is also concentrated in veins at the microscale.

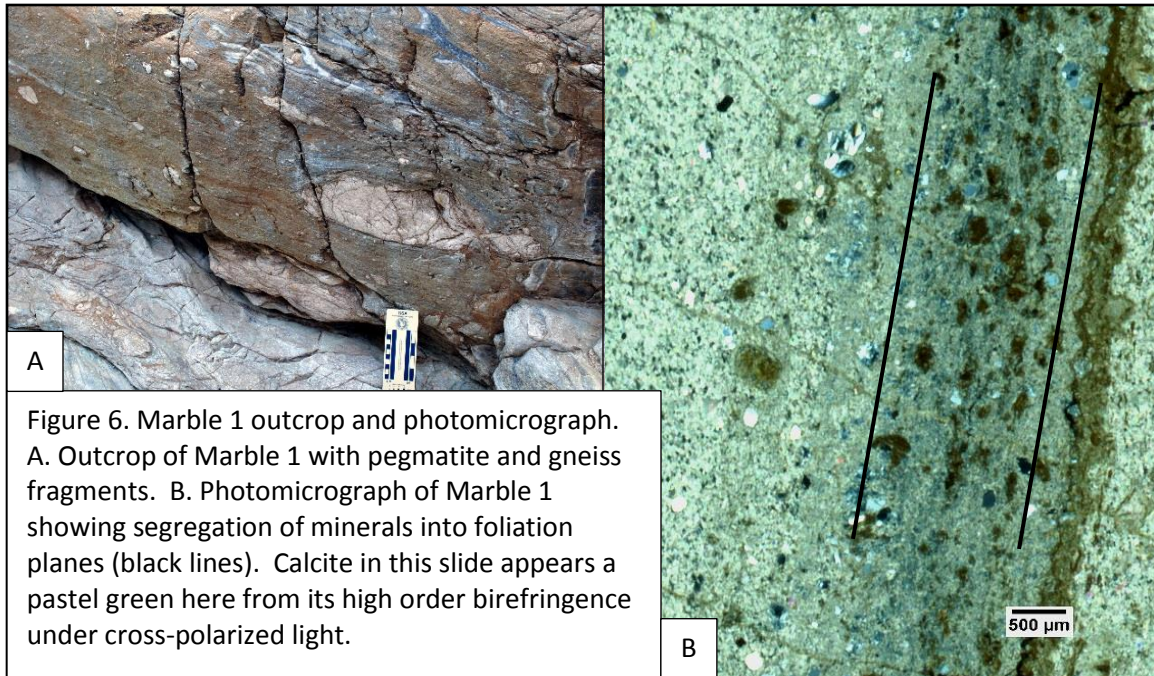
In the exposed shear zone, the gneiss is structurally above Marble 1. There is a sharp contact between the two elements. This contact is corrugated, with a wavelength of 10-15 meters and an amplitude of less than 1 meter. This contact is congruent with the thrust fault described by Miller and Friedman (1999). Some Marble 1 is also present above the gneiss, probably carried by the gneiss during thrusting. The contact with the upper Marble 1 is also sharp, with no mixing between the two units visible at the contact. Scattered fragments of gneiss can be found in Marble 1 away from the contact, and are tightly folded. How they were incorporated into the marble is not clear from field observations.

### *Marble Elements*

The marble portion of the exposed shear zone section consists of three elements based on each element's individual structures and mineralogy. Marble 1 displays the strongest foliation and is classified as a mylonitic *mélange* from the mixture of fragments and the presence of both brittle and ductile deformation. Marble 2 is further split into two elements, 2A and 2B. Compared to Marble 1, these elements are less foliated and contain less mixing of other elements. Marble 2A displays almost no foliation or lineations and is compositionally homogenous calcite. Marble 2B, by comparison, is strongly foliated and rich in micas, possibly talc or white micas. Despite their differences, Marbles 2A and 2B occur structurally at the same level within the shear zone, which is why they are grouped together.

### Marble 1

Marble 1 is a strongly foliated, calc-mylonite *mélange* found only in contact with



the mylonitic gneiss. An upper unit of Marble 1 extends from the top of the gneiss to the current, exposed surface of the turtleback. The Marble 1 below the gneiss is indistinguishable from the upper Marble 1, however, most of my work comes from investigating the lower unit.

The lower Marble 1 is approximately three meters thick, although there is some variation in this thickness. The matrix is dominated by very fine-grained calcite ranging from 20 micrometers to 200 micrometers in diameter, with most between 40 and 100 micrometers across. This fine-grained calcite forms the bulk of the mylonitic *mélange* in foliated layers ranging from 5 cm to less than a centimeter in thickness. Mineral segregation with almost pure calcite layers separated by thin layers of silica and other minerals defines the foliation plane. Mixed into this mylonitic texture are large fragments of other shear zone elements, including gneiss, pegmatite, marble, and diabase (Figure 6A). The size of these fragments covers a wide range from meter to sub-



millimeter scale. Over both canyons my field assistant and I observed 70 fragments in detail, and recorded their size and orientation within Marble 1.

The pegmatite fragments are the largest and most common, making up approximately 80% of the fragments in Marble 1. In terms of size, they range from about 10 cm to eight meters across, and are typically equant to slightly elongate in form. These fragments are brittlely deformed, with many fractures sub-perpendicular to the foliation of the host marble.

Gneiss fragments are much smaller and less common than the pegmatite, making up approximately 8% of the fragments observed. The gneiss fragments are typically 5 cm to 30 cm across their largest dimension. Typically, the gneiss fragments are stretched or folded into complex and asymmetric forms (Fig 5D). Compared to the massive gneiss, the fragments are dominated by darker minerals interlayered with thin silicic layers.

Marble fragments are also rare, making up approximately 12% of the observed fragments. Most are large fragments around a meter in diameter, but the absence of smaller marble fragments is possibly because I found them difficult to identify and differentiate them from the surrounding rock in the field. As a result, the percentage of marble fragments could be inaccurate.

The fragments observed were typically between 30 cm and 1 m across, and displayed fractures or veins that cut across them at sub-perpendicular orientations to each other. One set of these fractures was typically sub-perpendicular to the surrounding foliation, although a few exceptions were observed. Few samples from these fragments

could be reliably collected, but, from the thin sections produced, the grain size appears much larger than within the matrix. Grains size are on the scale of 50 to 100 micrometers with some smaller grains down to 10 micrometers, especially in veins.

Diabase fragments occur only at the micro scale, and only in one sample found near a young brittle fault that cuts the exposed shear zone. However, I am reluctant to classify this sample as a breccia, because the mylonitic layers in this sample include diabase fragments. Brecciated marble and gneiss occur in the young fault, but this marble sample was approximately 0.5 meters from the fault. This may suggest that the calcite was still deforming ductilely in areas even when brittle faulting was cutting portions of the shear zone.

Broken quartz grains were observed in some Marble 1 samples adjacent to pegmatite fragments. These quartz fragments are on the order of 70 to 400 micrometers in diameter and are sub-rounded and sub-equant in their form. It is not clear from observation what the source of the broken grains is. One possibility is that they are fragments from the pegmatite. The rounded form could then be the result of cataclasis. However, if the broken quartz grains predate metamorphism, then they could be from the protolith for Marble 1, which could have been a sandy limestone.

## Marble 2

Marble 2 consists of two sub-elements, Marbles 2A and 2B, which occur structurally in the same interval, but are distinct lithologically and of their internal structures.

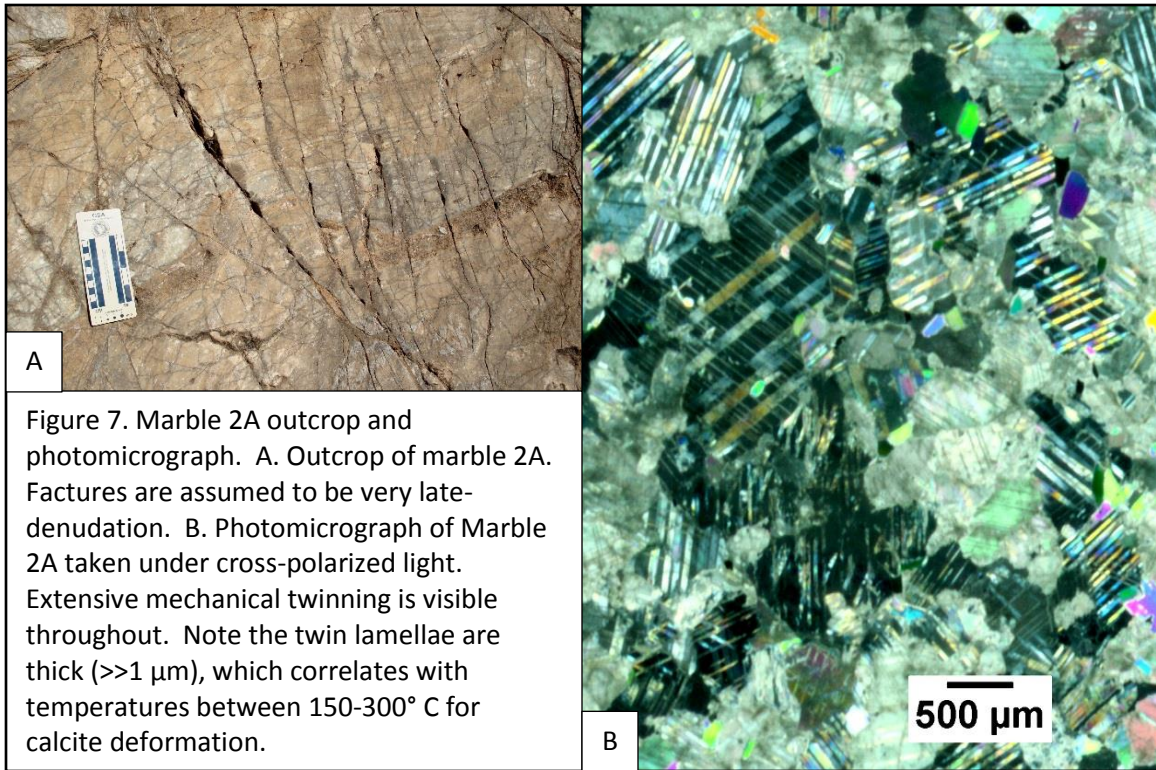


Figure 7. Marble 2A outcrop and photomicrograph. A. Outcrop of marble 2A. Fractures are assumed to be very late-denudation. B. Photomicrograph of Marble 2A taken under cross-polarized light. Extensive mechanical twinning is visible throughout. Note the twin lamellae are thick ( $>>1 \mu\text{m}$ ), which correlates with temperatures between 150-300° C for calcite deformation.

## Marble 2A

Marble 2A is a relatively unfoliated, crystalline-calcite marble structurally beneath Marble 1. The contact between these two units is indistinct to sharp. Contacts with Marble 2B are concealed in the field site. Where they are inferred, there is graded behavior observed in Marble 2A nearby, with fragments and increasing mica content towards Marble 2B. The thickness of Marble 2A is undetermined, as it extends below the exposed portion of the shear zone.

Mineralogically, Marble 2A is nearly all calcite, with trace grains of opaque minerals. Grains are coarse, ranging in size from 50 micrometers up to 2700 micrometers for their largest dimension, although most fall between 350 and 700 micrometers across. Most grains display one or two sets of mechanical twins, and are roughly equant in shape.

The twins themselves are characterized as thick, straight twins or type II twins (Burkhard, 1993). Twins range in thickness from 10 to 90 micrometers, with most approaching the upper limit of that range. Some thinner, type I twins (Burkhard, 1993) also exist, but are sparse. No other types of twins were observed.

## Marble 2B

Marble 2B is a strongly foliated, mica-rich, calc-mélangé at the base of the exposed portion of the shear zone. Structurally, it appears in the same interval as Marble 2A, but is spatially separate, with no direct contacts between the two observed. The contact between Marble 2A and 2B is inferred to be gradational, from observing increased mica in 2A near the inferred the contact. Contact with Marble 1 is also gradational. Unlike the contact with 2A, this contact is well exposed throughout the area where 2B is found. The dark and light brown bands of material in Marble 1 give way to almost entirely light-tan colored rock of Marble 2B over a span of less than a meter. Thickness of foliation layers is decreased from Marble 1, with layers taking on a thin, platy form in Marble 2B.

Everywhere Marble 2B is found, it is in contact with large exposures of pegmatite. In Canyon 2, in particular, pegmatite bodies or fragments up to 13 meters in length are in contact with Marble 2B. Foliation in Marble 2B wraps around the pegmatite, suggesting that the foliation is affected by the pegmatite. In adjacent canyons, large boudins of pegmatite on similar and larger scales are visible. This matches with the interpretation of Miller and Pavlis, that these are boudins (2005). The foliation of Marble 2B varies greatly in orientation around these fragments, following the surface of

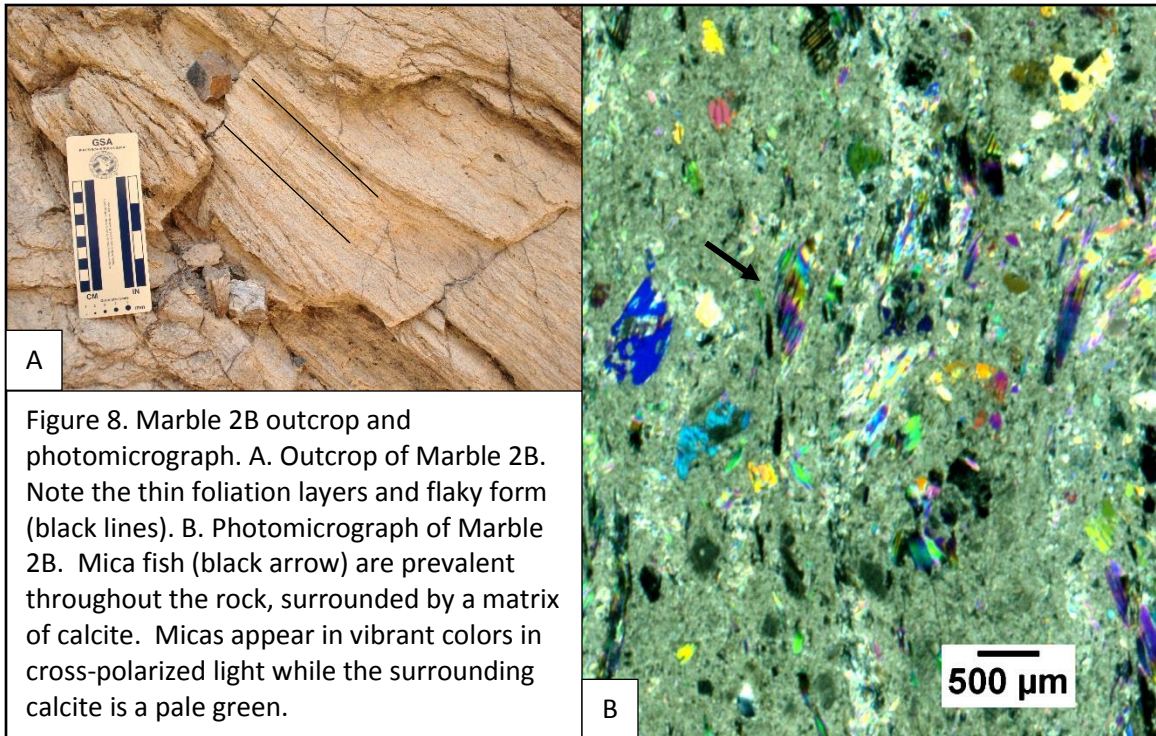


Figure 8. Marble 2B outcrop and photomicrograph. A. Outcrop of Marble 2B. Note the thin foliation layers and flaky form (black lines). B. Photomicrograph of Marble 2B. Mica fish (black arrow) are prevalent throughout the rock, surrounded by a matrix of calcite. Micas appear in vibrant colors in cross-polarized light while the surrounding calcite is a pale green.

the pegmatite. This causes the foliation of Marble 2B to deviate from those of the gneiss and Marble 1.

Mineralogically, approximately 20-25% of Marble 2B is a white mica mineral, possibly talc. However, the hand samples do not express a particularly soapy texture, which is a better identifier of talc than thin section observations (MacKenzie & Guilford, 1980). Total composition is approximately 20-25% white mica and less than 5% opaque minerals, with the remainder almost entirely fine-grained calcite. Calcite grains in this element range from 150 micrometers to less than 30 micrometers for their largest dimension. Smaller grains are certainly present, but are nearly unresolvable in the photomicrographs.

Lithic fragments are widespread throughout Marble 2B, of which approximately 80-85%, are pegmatite. The remainder are either gneiss or dolomite fragments.

Pegmatite and dolomite fragments display significant brittle deformation. Fragments of these elements display two sets of fractures, much like in Marble 1, with one set sub-parallel to shear-zone foliation and one set sub-perpendicular. Gneiss fragments present underwent accumulated ductile deformation, and form thin, folded shapes (Fig 5D).

Foliation of Marble 2B follows a similar plane to the foliation of the gneiss and Marble 1 elements, but often diverges in proximity to boulder-sized pegmatite fragments. This can be seen in Canyon 1, where foliations deviate from dipping northwest to abruptly changing to north and northeast dips. In Canyon 2, the surface of the pegmatite fragment in the middle of the canyon dips to the southwest, and so do the foliations of the adjacent Marble 2B outcrops. However, across the canyon to the north, Marble 2B dips closer to west, like most of the foliations throughout Canyon 2.

### *Pegmatite*

Throughout the shear zone, fragments of pegmatite can be found in all metamorphic elements. These fragments range in size from a centimeter up to 13 meters across. In the gneiss, the pegmatite can take the form of boudins, or as sills as described by Miller and Friedman (1999). However, in all other elements, fragments appear either as equant or slightly elongate from boulder-sized down to pebble-sized. The pegmatite can also appear as irregular fragments and boudins within the other elements. For the elongate fragments, the long axis is almost always sub-parallel to shear zone foliation. Irregular boulders are only found partially exposed at the very base of the canyons, and so it is impossible to determine an orientation.

There are no rooted intrusions of pegmatite in my field site. Even the largest



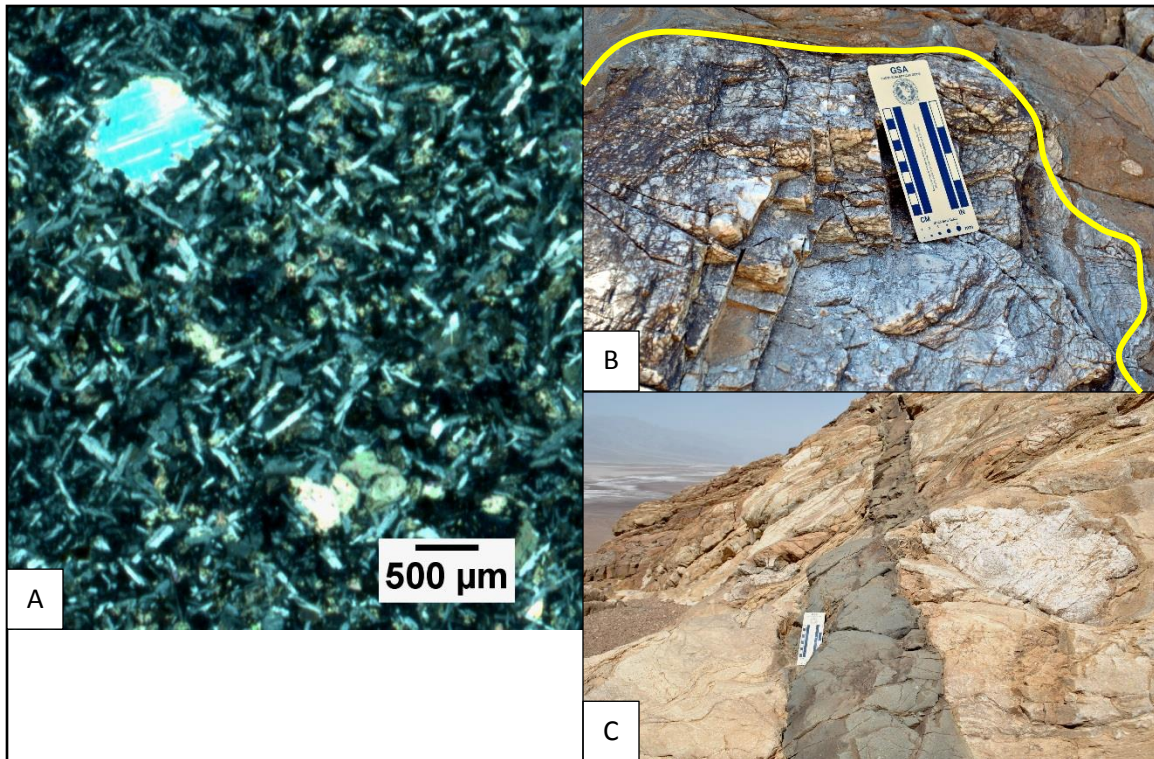


Figure 9. Diabase and pegmatite features. A. Photomicrograph of diabase sample. The large calcite grain in the top left is secondary. B. Pegmatite fragment in Marble 1, outlined in yellow. C. Diabase dike cutting rocks in canyon 2, looking northwest.

bodies are likely fragments, despite being partially buried. Other work on the Badwater turtleback has described sills and dikes of pegmatite, but the only at the deepest levels (Miller and Friedman, 1999). Additionally, there is no evidence of contact metamorphism with elements adjacent to the pegmatite in the field site.

Most pegmatite fragments observed display brittle deformation. This is visible both at the outcrop scale and at the micro scale. In outcrop, fragments show two sets of fractures, sub-perpendicular to each other, with one set sub-perpendicular to the general foliation of the shear zone. At the micro scale, most fractures are sub-perpendicular to the foliation. These microfractures are all filled with quartz or calcite crystals. Areas of crystal-plastic deformation are less common than fractures, but occur throughout

pegmatite fragments. They appear as mottled areas under cross-polarized light, and have very small grain sizes, with most less than 20 micrometers across. These mottled areas can be found around the edges of much larger grains, and are weakly foliated.

Mineralogically, the pegmatite is made mostly of crystalline quartz and feldspar. Calcite is present, but only where it has filled fractures as veins. Less than 5% of the pegmatite composition is opaque minerals.

### *Diabase*

Both canyons are cut by a mafic dike running from north to south. It is unknown if this is the same dike, as it does not extend to the uppermost surface of the turtleback between the canyons. Both dikes strike around north-northwest, but this is not enough to form a clear interpretation. The widths of these two dikes range from 30cm to 60cm. The dikes are geometrically planar, although some minor bends do occur. Some smaller, minor dikes are also present in the canyons. These smaller dikes only occur further east in the canyons and range from 3 to 10cm across. The largest of these can be seen on the map of Canyon 1 (Figure 3), but most were too small to include.

In thin section, the dikes mostly consist of plagioclase, chlorite and secondary calcite, with limited amounts of opaque minerals. The plagioclase grains are almost all thin and bladed, typically 400 micrometers long and 100 micrometers across. The plagioclase grains are randomly oriented throughout the rock. Calcite grains range from 200 micrometers to 2000 micrometers across, and are equant in shape. The largest calcite grains display sparse twinning. There are both type II twins and type III twins present in





Figure 10. Faults and Breccia. A. Faults, in blue, showing separation of element contacts in black from in Canyon 1. B. Brecciated zone of rock on at fault in Canyon 2, circled in red. Arrow points to most visible area of brecciation.

the calcite (Burkhard, 1993). Opaque minerals are around 150-200 micrometers across and equant in shape. These opaque minerals fill the remaining space, making up approximately 10-15% of the sample.

## Structures

Half a dozen faults cross both canyons at their western ends. These faults are relatively limited in their extent, disappearing under talus or lost in the steep cliffs of Marble 1 surrounding the canyons. Breccia occurs along some of the faults, with sharply angular fragments of marbles, pegmatite and gneiss, ranging from pebbles to fine sand in size. Photos of the faults and breccia can be seen in Figure 10A and B.

In both canyons, the faults are found clustered around outcrops of pegmatite. All the faults strike northeast, similar to the strike of foliations throughout the exposed shear zone. In Canyon 1, the four faults form two pairs of faults. These faults are sub-vertical in dip and show a vertical offset of approximately 40 centimeters for the northern-most pair, and 20 centimeters for the southern pair. As foliation layers and contacts are the only slip indicators present, I was unable to determine if there was any strike-slip

component. The magnitude of vertical offset decreased to no visible offset over a short distance, making identifying the faults difficult beyond just a few meters.

In Canyon 2, the northern most fault dips to the southeast at 42 degrees, and its exposure on the surface of the canyon marks the line of intersection with a sub-vertical fault that parallels the cliffs to the south. This fault contained breccia, with the fracture zone as wide as 8 centimeters in some areas. The breccia is cemented with coarse grained calcite 400 to 1000 micrometers in diameter. Fragments in the breccia range in size from less than 500 micrometers to pebbles and cobbles, which are easily visible in outcrop.

## CHAPTER IV

### METHODS

My study relies primarily on field work supplemented by thin section observations. In the field, mapping and foliation/lineation orientation data form the bulk of the information, along with detailed rock descriptions. There were some challenges in mapping the location, as many areas around the high canyon walls were inaccessible on foot. Mapping of these areas was supplemented by mapping on large-scale, aerial photographs generated using photogrammetry. For thin section analysis, I utilized both direct observation, with a petrographic microscope, and photomicrographs taken in both plane- and cross-polarized light to highlight grain boundaries and identify minerals and fabrics.

#### **Field Work**

Work in the field consisted of mapping the two exposed sections of the Badwater turtleback shear zone, measuring and documenting structures, recording the orientation of fragments, and describing the lithologic elements present in detail. In particular, I focused on collecting the strikes and dips of foliation planes, mineral lineations, orientation of faults and fractures, the distribution of fragments in mélangé, and spatial relations between these elements.

Mapping the two canyons was problematic, as steep cliffs prohibited directly walking some areas. To supplement this, I collected approximately 800 photographs per canyon for use in constructing three-dimensional models of the canyons using a

technique called photogrammetry. In an automated photogrammetry program, such as AGISoft's Photoscan, the software matches similar features in each photograph to construct a three-dimensional model of the subject. This process requires a thoughtful approach to photography. To help the program construct the three-dimensional model, the same landmarks must be present in many of the photographs taken. Using this model, I located lithologic contacts that were visible, but otherwise inaccessible. This method was helpful in improving the precision of my map versus mapping on satellite and aerial photos alone, which lacked sufficient detail for the scale of my work.

For the foliations and lineations, I took a total of 40 measurements. The measurements are distributed across both canyons in three lithologic elements. Measurements were densely concentrated compared to larger-scale mapping projects, with measurements typically separated by 10 meters or less. The three elements I measured are the gneiss, and Marbles 1 and 2B. The measurements from Marble 2B varied greatly from the other two elements, seemingly affected by the proximity of pegmatite clasts. I chose not to include them in my final stereonet plots, as I felt they were not representative of the foliation of the exposed shear zone as a whole. Lineations were also measured where visible, mainly in the gneiss and Marble 1. A table of foliation and lineation measurements can be found in Appendix A: Foliations and Lineations.

The fractures I measured include faults that cut the shear zone and fractures in fragments within the *mélange*. The fragment fractures were measured to show a relationship between the ductile strain surrounding the fragments and the brittle fractures cutting the fragments. These fractures all terminated at the edges of the fragments. Typically, each fragment had one or two sets of fractures and one measurement was

taken for each set. The fragments chosen were largest fragments, most measuring at least 30cm across for their smallest dimension. This minimum was chosen for ease of taking an accurate strike and dip measurement. Smaller fragments were not large enough to take a reliable strike and dip measurement, even with an aid, such as a clipboard. Measurements came from a total of 70 fragments across both canyons in three lithologic elements, primarily in Marble 1, but also in the Gneiss and Marble 2B.

Foliations, lineations and fractures were analyzed using Orient 3.3 (Vollmer, 2015). To calculate mean values and 95% confidence intervals, a bootstrap error calculation included in the program was run with 1000 iterations (DiCiccio and Efron, 1996).

A total of 33 fist-sized or smaller samples were taken over the course of study. This number is in accordance with limits set by permit DEVA-2016-SCI-0014, which allowed for the collection of up to 40 samples in Death Valley National Park within the study area. Samples were taken from each of the six lithologic elements. Samples were oriented using foliation surfaces on the sample, or by some other, not structurally significant surface if foliation surfaces were not usable or present. A list of samples collected accompanied by brief descriptions can be found in Appendix B: Samples.

### **Thin Sections**

Thin sections were cut from each of the 33 samples taken from the field. Most sections were cut perpendicular to the foliation plane measured from the Gneiss and Marble 1, and parallel to the lineation within that plane, approximately N60W, and then mounted, so that when placed under a petrographic microscope, the observer is looking

structurally up. Six thin sections were cut perpendicular to lineation and foliation, in a plane striking N30E, in six samples. These were produced either because structures were unclear in the sample, or to compare the two planes for strain analysis. A table of thin sections along with their orientation and a brief description are available in Appendix C: Thin Sections.

### **Strain Analysis**

To perform a strain analysis of the calcite marbles, I considered several methods. From observations of the thin sections using a petrographic microscope, I sought to identify strain makers, such as strain shadows around porphyroclasts, areas of recrystallization, such as bulging or grain boundary migration, and changes in grain size, where a reduction in average grain size could indicate increased strain accommodation (Hirth and Tullis, 1992). To aid in identifying these features, photomicrographs were taken of sections from each of the three marble elements. This was done both with a petrographic microscope mounted digital camera and with a high-resolution flatbed scanner with polarized filter inserts. Due to the very small grain sizes for calcite in Marble 2B, a thorough strain analysis was not possible, but analyses for both Marble 1 and 2A were feasible.

Portions of the photomicrographs were also used in a finite strain analysis. I investigated several methods of strain analysis that could be applied to calcite. These include calcite twin strain gauges (Groshong, 1976; Groshong et al., 1984), pole figure and slip plane analysis using electron backscatter diffraction (EBSD) (Wright S., 2011; Pryor et al., 1999), and grain center-to-center strain analysis, also known as the Fry

method (Fry, 1979; Mulchrone et al. 2003; Waldron et al. 2007). Initially, I pursued EBSD, but it proved unfeasible and I instead opted for an analysis based on the Fry method.

The Fry method works on the assumption that the spatial distribution of mineral grains in a rock sample is not random, and that grain distribution patterns with a degree of ordering carry information (Fry, 1979). Consider a theoretical rock with a completely random distribution of grains. This rock would have no ordering, so the distribution would be isometric. However, as a homogenous strain is applied, each grain is affected, and their distribution becomes more ordered. This ordering can be expressed as clustering or anticlustering of grains within a sample, with anticlustering being more common in rocks (Fry, 1979).

Given that the Fry method assumes the distribution of grains in a rock will show anticlustering as the rock undergoes homogeneous strain, the rock grains can then be analyzed using a graphical or numerical method (Fry, 1979; Waldron et al., 2007; Mulchrone et al., 2013). This analysis method has been improved since the Fry method was first introduced by development of the normalized Fry method, the enhanced normalized Fry method (ENFry), and the Delaunay triangulation method (Erslev, 1988; Erslev and Ge, 1990; Mulchrone, 2003). The program used for my strain analysis is based on the Delaunay triangulation method, which has been shown to be less subjective than previous methods and less laborious to implement (Mulchrone, 2003; Mulchrone et al. 2013).

The analysis works by comparing the distance between the centers of objects in a two-dimensional plane while normalizing for the different sizes of the objects. The normalized distances to an arbitrary grain center are then plotted as a point. This point shows both the orientation of the two points, relative to the plane axes, and the distance, as distance from the center of the plot. This process is then repeated for all grains, yielding the Fry plot (Fry, 1979; Erslev, 1988). As the plot is generated, an ellipse should take shape from the nearest neighbors to each arbitrary point. Fry and other workers have shown that this ellipse, along with the total distribution of grains in the plot, can be used to generate and fit a finite strain ellipse equivalent to the strain accommodated by the sample (Fry, 1979; Erslev, 1988; Mulchrone, 2003).

For my analysis I used two programs. ImageJ was used to identify grain sizes and distribution, while a script written by Mulchrone et al. for Wolfram Mathematica was used to produce the Fry plots and derive a finite strain ellipse from those plots (2013). To prepare the photomicrographs for this process the grains of calcite were traced in black using a photo editing program, such as Microsoft Paint or Adobe Illustrator. Then the original image is removed, and the trace placed on a white background. Once this is done, the image can be imported into Mathematica, where the analysis is performed. The scripts used do not always work flawlessly, and require that spurious grains be removed manually before completing the analysis. The largest dimension of each grain used was recorded for use in grain size distribution as well.



## CHAPTER V

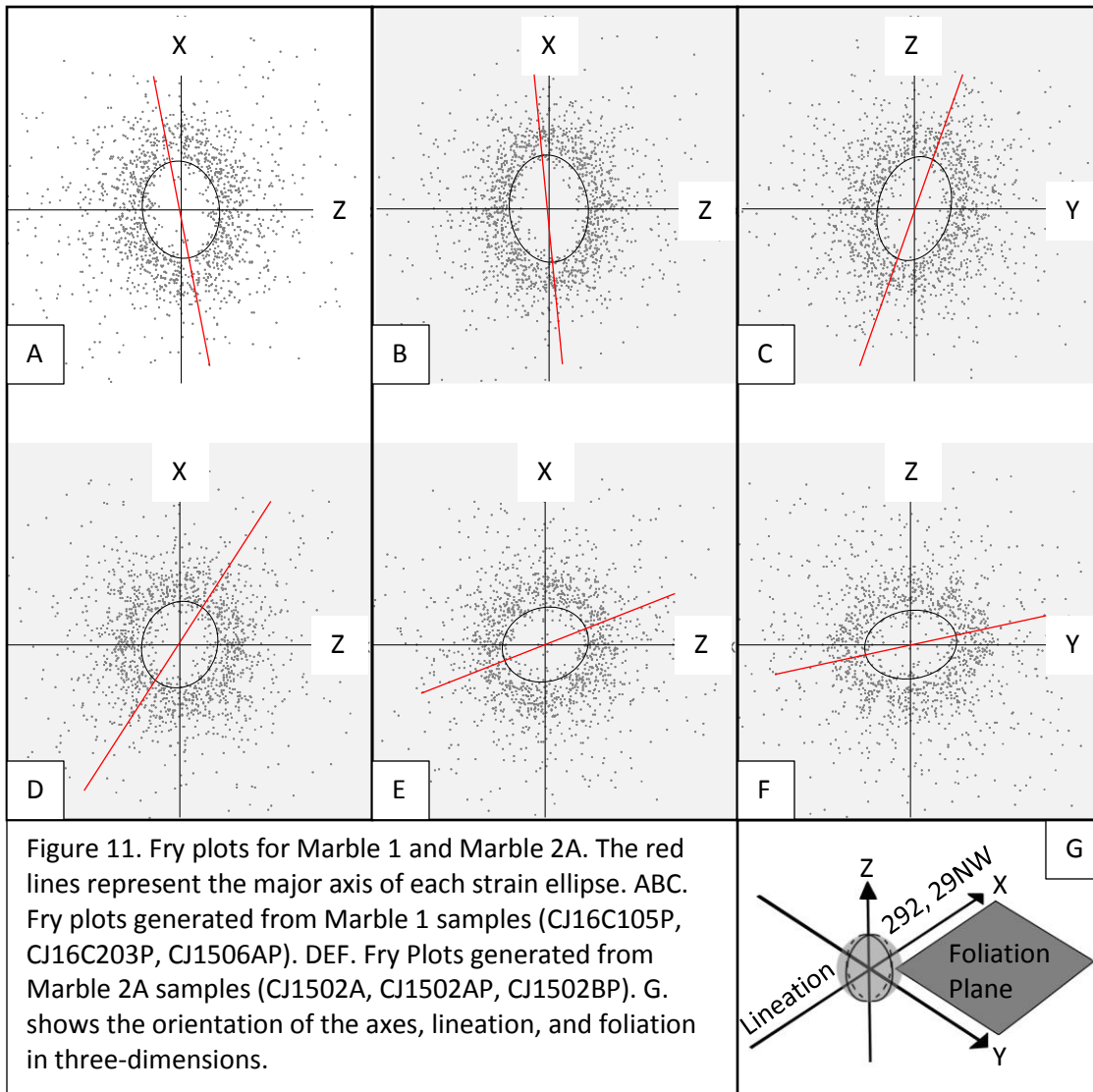
### RESULTS

The results shown here are the product of the strain analysis, grain size distributions, and foliations and fractures measured. Each section details how to read these data; and interpretations of the data follow in chapter six.

#### **Strain Analysis**

The results of the strain analysis are shown both with Fry plots and grain size distributions. Figure 11 shows the Fry plots for Marbles 1 and 2A. The first two panels of Marble 1 (Fig. 11: A, B) and Marble 2A (Fig. 11: D, E) represent Fry plots and strain ellipses in the X-Z plane. Each panel shows the Fry plot generated from a different sample. Multiple samples are plotted to compare for consistency. The last panel of each row represents the Z-Y plane, Fig. 11C for Marble 1, and Fig. 11F for Marble 2A. Each Fry plot also includes a red line to illustrate the major axis of the strain ellipse. Panel G illustrates the relation of these different views to the foliation and lineation in each sample.

The X-Z plane shows the finite strain ellipse in the plane perpendicular to foliation and parallel to lineation. This plane is important as it should capture the maximum stretching direction in the sample. This allows us to correlate the axis of maximum finite stretch with the longest dimension of the resulting ellipse in the Fry plot (Hirth and Tullis, 1992). The maximum finite stretch axis and its orientation can be correlated with sense of shear, which is discussed in detail in Chapter VI, and the next



page shows that, for at least Marble 1, this analysis is possible. The Y-Z plane is included to explore the intermediate strain axes, and can help visualize the strain accommodated in three dimensions.

By adding the ellipse on the Y-Z plane, perpendicular to the X-Z plane, we can visualize a very rough, finite strain ellipsoid. However, this information can only give us a glimpse of the final sum of the strain accommodated, and tells little about the rate or individual events that created this final state without further correlations (Erslev, 1988).

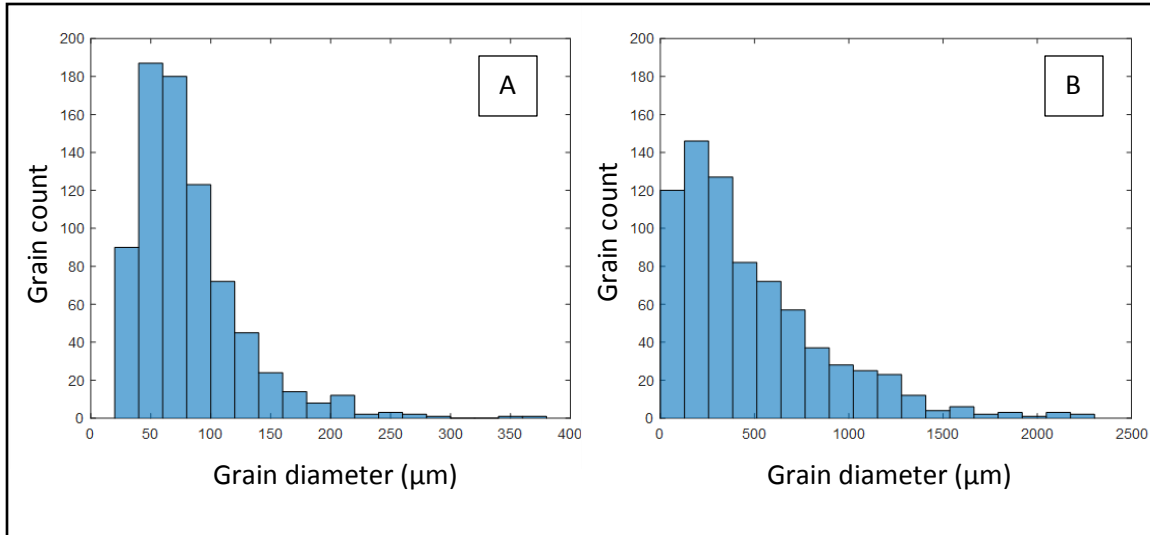
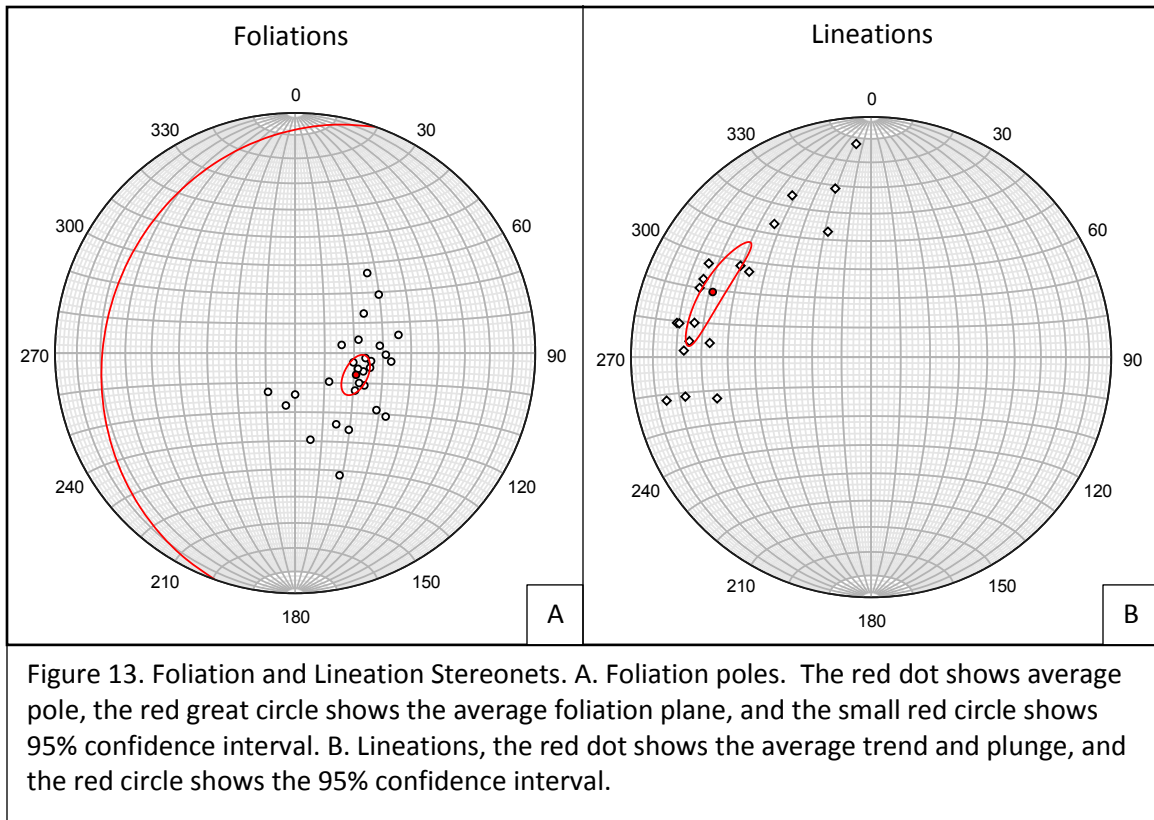


Figure 12. Calcite grain size distributions. A. Marble 1, each box has a range of 20 micrometers. B. Marble 2A, each box has a range of 125 micrometers.

Small grain size can be correlated with increased strain accommodation. The entire range of grains in the Marble 1 plot would fit in the first three boxes of the Marble 2A plot. Relative to each other, Marble 1 must have experienced more strain in its deformation history.

In Figure 11A and B, Marble 1 shows an asymmetry. That is, the major axis of the strain ellipse is angled away from the foliation plane. In this instance, the axis is rotated counter-clockwise away from the X-axis. Note that this does not necessarily mean that the rock material was rotated in this way. Dynamic grain recrystallization realigns grains by movement of grain boundaries (Hirth and Tullis, 1992). Interpretations as to the significance of the asymmetry are covered in chapter six.

Asymmetry is also visible in Fig. 11C, with clockwise rotation away from the Z-axis. For Marble 2A asymmetry is present, but it is not consistent between the two samples in the X-Z plane. Fig. 11D is rotated clockwise away from the X-axis a small amount, but Fig. 11E shows a larger rotation towards the Z-axis, also in a clockwise direction. Fig. 11F shows a large angle rotation from the Z-axis towards the Y-axis.



### Grain Size Distribution

The histograms of Figure 12 compare grain size distribution between Marble 1 and Marble 2A. Using the same grain-trace images used to generate the Fry plots, the longest dimension of each grain was measured in micrometers and plotted to build Figure 12. Figure 12A shows that grain sizes in Marble 1 range from 20 micrometers up to 375 micrometers across, with most between 50 and 125 micrometers across. By comparison, Figure 12B shows a much wider distribution of grain sizes, from 40 micrometers up to 2250 micrometers across. Most grains, however, are between 125 and 375 micrometers across. For some perspective, most of the distribution of Marble 1 would fit in the first box of Figure 12B, and the entire range of Marble 1 grains would fit in the first three boxes of Marble 2A's distribution.

## Foliation and Lineation Orientations

All field measurements of relevant foliation and lineation orientations are plotted in Figure 13. Figure 13A shows the foliation measurements taken from both canyons from the gneiss, Marble 1 and Marble 2B. Some Marble 2B foliations were discarded as outliers. The 28 foliation poles are shown on the figure give an average foliation plane orientation of  $199^{\circ} 21\text{NW}$  (N19E, 21NW). The red ellipse on Figure 13A is the 95% confidence interval, determined by a bootstrap error calculation, with a parameter of  $1000 = N$  for the number of resamples. This bootstrap error calculation is included in the Orient 3.3 program used to generate the stereonet (Vollmer, 2015).

Figure 13B shows the orientation of mineral lineations measured alongside foliations. Most measurements come from gneiss outcrops, where lineations are clearly visible. Some outcrops of Marble 1 also featured visible lineations and are shown here. Marble 2B, despite showing foliation does not visibly show lineations and so none of the measurements shown come from Marble 2B. The mean trend and plunge across all measured lineations is  $292^{\circ} 29\text{NW}$  (N68W 29). All lineations are sub-parallel to foliation dip on the outcrops where they were measured. A 95% confidence interval is shown as a red ellipse, and was generated by the same parameters as the foliation confidence interval.

## CHAPTER VI

### DISCUSSION AND CONCLUSION

The accommodation and partitioning of strain into different lithologic elements throughout the exposed shear zone can be framed temporally within the denudation of the Badwater turtleback. The observations and results show a clear progression of deformation mechanisms in both the quartz and calcite within the shear zone. In the quartz there is a trend from sub-grain rotation to bulging and cataclasis, while in the calcite the progression follows the intensity of grain size reduction and twinning. Both trends correlate with a cooling of the shear zone during exhumation.

Concurrently, strain distribution within the shear zone partitions strain into different lithologic elements. During denudation of the shear zone, strain departs from the gneiss and is then accommodated across the marble elements. Additionally, the significance of the relatively low amount of deformation in Marble 2A is explored in this chapter. My interpretations are further correlated with previous studies to build a history of deformation as the Badwater turtleback passes through the brittle-ductile transition.

#### **Deformation Mechanisms**

Deformation mechanisms are the best proxy for strain and temperature conditions within the shear zone. In quartz and calcite, the style and intensity of crystal-plastic deformation can be correlated with the conditions of deformation. Intensity, which is defined as the prevalence of crystal-plastic deformation throughout a sample, can be correlated with the magnitude of strain accommodation. Assuming constant strain rate

and sufficient heat, as the magnitude of strain increases, crystal-plastic deformation manifest as grain size reduction becomes more prevalent (Burkhard 1992, Stipp et al., 2002; Rogowitz et al., 2014). Additionally, in both quartz and calcite, their different styles of deformation are ordered by temperature. Identifying the preferred style of deformation in each allows a correlation with temperature (Hirth and Tullis, 1992; DeBresser et al. 2002). When this connection between deformation mechanism and environment is established, I can then further correlate the deformation environment with the progression of the shear zone through the brittle-ductile transition.

### *Quartz Deformation*

Within the gneiss, quartz is the diagnostic mineral for deformation. During crystal-plastic deformation there is a well-defined hierarchy of mechanisms and mineral assemblages associated with quartz. Evidence of two crystal-plastic mechanisms can be observed in Figure 5B: bulging and sub-grain rotation. In addition, chlorite is present in the gneiss, which can be seen in Figure 5C. These three features are important clues in describing the deformation progression in the gneiss.

Comparing my observations to the quartz recrystallization model developed by Stipp et al. (2002), the highest temperature mechanism in the gneiss is sub-grain rotation, which occurs between 400 and 500° C. However, the mineral assemblage suggests that the temperatures seen in the preserved deformation did not reach 500° C. According to Stipp et al., at these temperatures, the formation of muscovite and biotite are expected to accompany sub-grain rotation in quartzofeldspathic shear zones (2002). However, within the exposed Badwater turtleback shear zone, the gneiss contains small amounts of

muscovite and biotite relative to the model described by Stipp et al. (2002). This constrains the highest temperature quartz deformation to the low end of sub-grain rotation, around 400° C. Additionally, the relative scarcity of preserved sub-grain rotation also supports this interpretation.

Moving down in temperature, the final crystal-plastic deformation mechanism seen in quartz is bulging. Referring back to Stipp et al., bulging occurs between 280 and 400° C (2002). At the higher end of the bulging regime, the expected mineral assemblage is chlorite and potassium-rich feldspar. Compared to sub-grain rotation, bulging is more commonly observed, and chlorite is clearly visible in many samples along with feldspars (See figure 5C).

Below temperatures of 280° C, quartz does not easily deform crystal-plastically, and deformation transitions into brittle mechanisms. Yet, there is little evidence of cataclastic flow. Some of the larger grains of quartz in the gneiss have microfractures. However, the surrounding texture suggests only ductile flow and not cataclastic flow, so the significance of these microfractures to the quartz deformation is unclear. It would appear that significant quartz deformation ceased once temperatures dipped below 280° C.

My interpretation is that the highest grade of metamorphism experienced by the quartz took place around 400° C, high enough to produce a mixture of bulging and sub-grain rotation, and the correct mineral assemblage. However, this only represents the last stage of deformation in the quartz. If any higher-grade metamorphism had existed, it may have been overprinted and there would be no record preserved. Another possibility



is there was no higher-grade metamorphism to be preserved. Regardless, this last gasp of quartz deformation still contains important data.

### *Calcite Deformation*

In the marbles and calc-mylonite mélange, calcite twinning can be correlated with temperature of deformation below 400° C (Lacombe, 2010). However, above 250° C, dynamic recrystallization is also an important factor present (Ferrill, 1998). Both mechanisms are significant to calcite deformation in the exposed Badwater turtleback shear zone.

For twinning, the twin width and density are the primary means of temperature correlation. The width of twins in calcite is proportional to temperature, and the density of twins is inversely proportional to temperature (Lacombe, 2010). In comparison, dynamic recrystallization of calcite is correlated with the relative amount of strain accommodated, and a minimum temperature of 250° C (Rogowitz et al. 2014). Within the exposed Badwater turtleback shear zone, grain size reduction is the primary result of dynamic recrystallization.

Marbles 1 and 2B both consist of fine-grained calcite, and no readily-apparent twins. Most likely these units both accommodated significant strain while at temperatures above 250° C. However, the lack of twins does not preclude further deformation at lower temperatures. At low temperatures, twin width can decrease in thickness to less than one micron across (Groshong, 1972; DeBresser et al., 2002). These microtwins may not have been resolvable optically, but Burkhard presents several examples in his 1992 paper that, even in grains down to 1 micron across, twinning can

	type I	type II	type III	type IV
<b>Geometry</b>	- thin twins	- thick (>>1 $\mu$ m)	- curved thick twins	- thick, patchy
<b>Description</b>	- straight - rational - 1, 2 or 3 sets per grain	- straight - slightly lense shaped - rational	- twins in twins - completely twinned - irrational	- sutured twin boundaries - trails of tiny grains - irrational
<b>Interpretations</b>	- little deformation - little cover - very low temperature - (post-metamorphic) - (late tectonic)	- considerable deformation - completely twinned grains are possible - syn- or post-metamorphic deformation	- large deformation - intracrystalline deformation mechanisms (r- & f-glide) - syn-metamorphic deformation.	- large deformation - dynamic recrystallization (grain boundary migration) - pre- or syn-metamorphic deformation
<b>Temperature</b>	< 200°C	150-300°C	> 200°C	>250°C

Figure 14. Types of calcite twins from Burkhard (1992). Most twins in Marble 2A are type II.

still easily occur, and can be observed with an electron microscope. Microtwins can even accommodate twins to temperatures below 150 C (Kennedy and White, 2001). With that example, it is possible for Marbles 1 and 2B to initiate crystal-plastic deformation at the same time as the quartz, both through dynamic recrystallization and twinning, and then continue deformation long after the quartz stopped deforming.

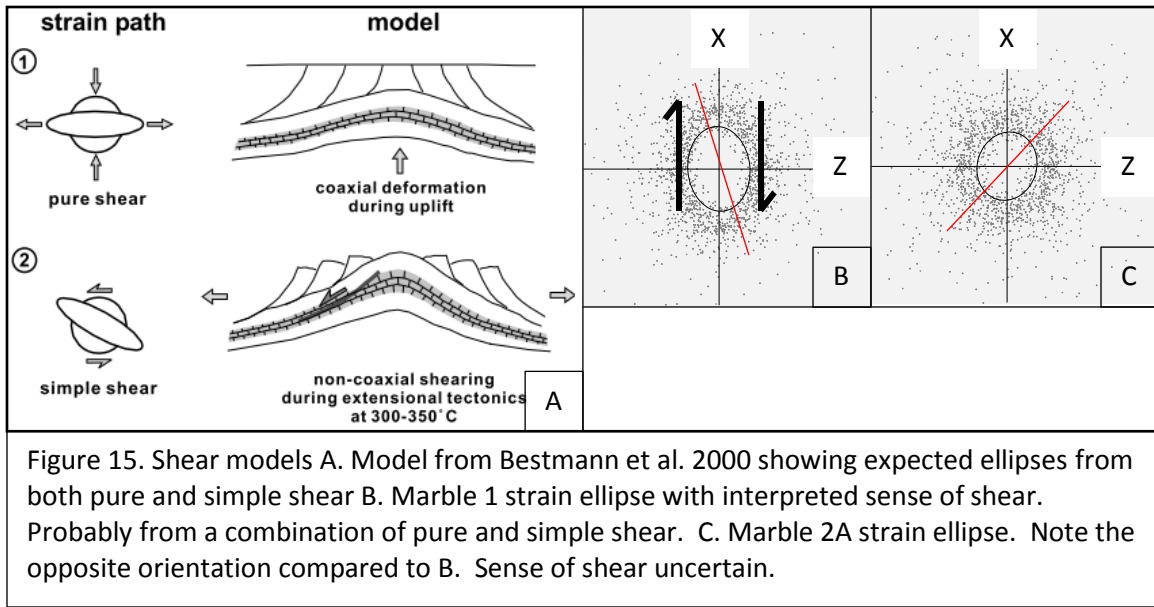
In contrast, Marble 2A displays only large grains and thick twins, meaning the twins are much greater than 1 micron across. According to Burkhard's twin classification in Figure 14, Marble 2 shows Type II twins (1992). Type II twins occur at 150-300° C, a range of temperatures mostly below the boundary for dynamic recrystallization. If we assume that the temperatures experienced by Marbles 2A and 2B were the same while the shear zone was exhumed, then there must be a different reason that the two lithologic elements do not express the same deformation style.

The difference in deformation may be the result of the pegmatite present in the shear zone. Marble 2B features numerous boulder-sized fragments of pegmatite. These pegmatite fragments are mainly quartz and feldspar, which are rheologically much

stronger than the calcite surrounding them (Miller, 1992). Most strain experienced by Marble 2B around the pegmatites could be partitioned to the surrounding calc-mylonite, because it would be weaker than the pegmatite and can still deform in a crystal-plastic manner at low temperatures.

Another factor in the comparison between Marbles 2A and 2B is the presence of white mica in Marble 2B. The white mica is likely talc, which may have originated in a metamorphic reaction between dolomite in the marbles and silica from the pegmatite (Bowen, 1940; Weeks, 1956; Gordon and Green, 1970; Eggert and Kerrick, 1981). Regardless of the exact mineral, mica minerals are weaker than calcite, and glide along their cleavage planes is easier to initiate than twinning (Lister and Snoke, 1987). The combination of weak rheology and proximity to strong materials most likely accounts for the difference in deformation between Marble 2A and 2B. However, Marble 2A still accommodated some strain, as twinning is present, but the amount of strain accommodated must be relatively less than in Marble 2B.

The relatively small amount of strain accommodation in Marble 2A is further supported by the Fry plots. In Figure 15, the strain ellipse for Marble 1 shows a good correlation with models for a progressively sheared calcite described by Bestmann et al. (2000). In progressive simple-shear or non-coaxial shear, the axis of maximum finite stretch is rotated closer to the direction of extension as more strain is accommodated (Lister and Snoke, 1984; Wenk et al., 1987). For this analysis, the X-axis, which is parallel to lineation, represents the extension. In Figure 15B, the finite strain ellipse generated for Marble 1 fits the predicted model and the sense of shear is top to the NW, matching observations from the field. In contrast, the ellipse generated from Marble 2A



in Figure 15C is relatively equant, and the axis of maximum finite stretch is further from the axis of extension. Since Marble 2B is mylonitic, like Marble 1, the comparison between 2A and 2B is the same. More strain is accommodated in Marble 2B than in 2A.

One caveat to this interpretation is that the finite strain ellipse generated from the Fry plots carry no information about strain magnitude (Fry, 1979). Without additional information, it is not be possible to determine whether Marble 1 or 2A accommodated greater strain. Considering the preceding interpretations, the likelihood of Marble 2A accommodating more strain is low.

A more objective analysis of the finite strain ellipse comparison is that the finite strain ellipse may not show enough stretch for Marble 2A. The Fry method, and its subsequent iterations, only compares the center-to-center relationships to generate the Fry plot (Mulchrone et al. 2002). For this investigation, only the whole grains were considered for generating the Fry plot. Including twins in the Fry plot was not appropriate, as it is unproven if their spatial distribution is significant for strain analysis.

Therefore, the finite strain ellipse generated from the Fry plots does not reflect the strain accommodated by twinning.

Based on these interpretations, the Marble elements of the shear zone express a later stage of deformation than the quartz. The progression of deformation goes from dynamic recrystallization in Marbles 1 and 2B, and continues to mechanical twinning as temperatures drop lower than needed for crystal-plastic deformation in the quartz. This interpretation solidifies the marble elements as the last stage of ductile deformation in the shear zone.

### **Strain Partitioning**

With an understanding of the deformation of each element, it is possible to piece together a history of strain partitioning into different lithologic elements over time as the shear zone as was exhumed. Before passing the brittle-ductile transition for quartz, temperatures peaked at  $\sim 400^{\circ}\text{C}$ . Sub-grain rotation occurred in quartz at this stage, and chlorite was produced in the gneiss. Concurrently, deformation in the Marbles 1 and 2B was accommodated by dynamic recrystallization, and grains in Marble 2A twinned. At this stage strain throughout the shear zone is accommodated crystal-plastically by all elements present.

Holm's thermochronology work determined that the Badwater turtleback crossed the  $350^{\circ}\text{C}$  isotherm at approximately 24 Ma (1992). This marks the starting point for the shear zone moving into the brittle-ductile transition. However, the first stage of the transition would take some time, as the shear zone would not cross the  $300^{\circ}\text{C}$  isotherm until  $\sim 13$  Ma (Holm et al. 1992).

As the shear zone began to cool, quartz ceased sub-grain rotation and deformed only through bulging. The marble elements continued to deform as before, accommodating more strain as the capacity for strain accommodation in the quartz was diminished. However, once the shear zone passed the critical 280° C isotherm, ductile deformation only continued in the marble.

Dioritic dikes in the core of the Badwater turtleback have been dated to  $6.3 \pm 0.2$  Ma by Holm (1992). Miller (1991) observed that these dikes are syn-kinematic with late-stage faults within the turtleback. This observation constrains the transition from ductile to brittle transition. This means that the shear zone was entirely within the brittle regime for quartz by 6.1 Ma at the latest. This transition may have occurred earlier, as the dikes are far deeper in the turtleback than the exposed shear zone, which sits near the surface of the turtleback.

However, the marble elements of the shear zone must have continued ductile deformation past the transition to brittle deformation for quartz. Since there are fragments of the gneiss in Marble 1, the marble must have been actively deforming to incorporate the fragments. All strain must have been partitioned into the marbles by this point, as there is no cataclasis or faulting to indicate any movement within the gneiss.

Some brittle deformation did occur in the pegmatites during this time. Fractures sub-perpendicular to the foliation in the surrounding calc-mylonite suggest a kinematic connection. These fractures may have opened in response to extension of the shear zone (Atkinson, 1987).

The last stage of deformation occurred in one of the marble elements, although which one is unclear. After 4 Ma, the opening of the modern Death Valley had begun, and the Badwater turtleback was fully exhumed (Knott et al. 2005, Miller, 2005). If there was any further ductile deformation between 6.3 and 4 Ma, it must have occurred within the marble and would have been restricted to twinning.

## **Conclusions**

In summary, with all the data collected and analyzed, I have related the partitioning of strain within the Badwater turtleback to a timeline of exhumation. Observations from the field indicate that the marble elements of the shear zone were the last to deform ductilely. Fractured fragments of pegmatite confirm that the marbles continued to deform after the shear zone had cooled beyond the bounds for crystal-plastic quartz deformation. Passage of the shear zone through the ductile-brittle transition can be constrained between 13 and 6.3 Ma for both quartz and calcite.

Within the marbles, a further partitioning of strain can be seen in several observations. Grain sizes are much smaller in Marble 1 and 2B, compared to Marble 2A. Additionally, both Marble 1 and 2B are strongly foliated, while Marble 2A shows no foliation. In comparison, Marble 2A is relatively undeformed and features only type II twinning (Burkhard, 1992).

Strain analysis using an adaptation of the Fry method also shows more progressive deformation in Marble 1 than in Marble 2A. The analysis matches field observations, indicating a top to the northwest shear in the footwall of the Badwater

turtleback shear zone, which can be seen in the orientation of porphyroclasts within the gneiss.

I recommend that future strain analysis in the Badwater turtleback expand upon the strain analysis in this report. Only Marbles 1 and 2A were analyzed with Fry plots. Investigation of the gneiss, pegmatite and Marble 2B could add significant understanding to the accommodation of strain in this shear zone. A more efficient approach than the Fry method would be to use Electron Backscatter Diffraction to obtain full orientation maps for use in strain analysis. This would allow all deformation mechanisms, including twinning, to be considered in full.



## APPENDIX A

### FOLIATIONS AND LINEATIONS

Foliation				Lineation	
Canyon	Element	Azimuth	Quadrant	Azimuth	Quadrant
2	Marble 2B	132, 37SW	N48W 37SW	-	-
2	Marble 1	185, 33NW	N5E 33NW	275, 33	N85W, 33
1	Marble 2B	305, 16NE	N55W 16NE	-	-
1	Marble 1	191, 26NW	N11E 26NW	281, 26	N79W, 26
2	Marble 2B	175, 29SW	N5W 29SW	-	-
1	Marble 1	205, 26NW	N25E 26NW	292, 24	N72W, 24
1	Marble 1	215, 34NW	N35E 34NW	215, 34	S35W 34
1	Gneiss	270, 14N	N90W, 14N	356, 12	N4W 12
1	Gneiss	260, 30NW	N80E, 30NW	348, 29	N12W 29
1	Marble 1	215, 38NW	N35E 38NW	305, 38	N55W 38
1	Gneiss	235, 32NW	N55E 32NW	324, 32	N36W 32
1	Gneiss	250, 45NW	N70E, 45NW	341, 44	N19W 44
1	Marble 2B	280, 18NE	N80W, 18NE	-	-
1	Marble 1	212, 24NW	N32E 24NW	300, 23	N60W 23
2	Gneiss	168, 22SW	N12W 22SW	258, 22	S78W 22
2	Marble 2B	195, 24NW	N15E 24NW	-	-
2	Gneiss	170, 36SW	N10W 36SW	255, 34	S75W 34
2	Gneiss	186, 26NW	N6E 26NW	275, 25	N85W 25
2	Marble 2B	181, 31NW	N1E 31NW	-	-
2	Marble 2B	220, 15NW	N40E 15NW	-	-
2	Gneiss	184, 24NW	N4E 24NW	272, 23	N88W 23
2	Gneiss	194, 22NW	N14E 22NW	280, 20	N80W 20
2	Marble 1	170, 16SW	N10W 16SW	258, 14	S78W 14
2	Marble 1	189, 20NW	N9E 20NW	280, 19	N80W 19
1	Marble 1	240, 28NW	N60E 28NW	334, 26	N26W 26
2	Marble 2B	150, 27SW	N30W 27SW	-	-
2	Marble 2B	145, 35SW	N35W 35SW	-	-
2	Gneiss	205, 24NW	N25E 24NW	295, 24	N65W 24

## APPENDIX B

### ROCK SAMPLES

Sample	Can.	Element	Oriented Surface	Notes
CJ15-01	1	Gneiss	N10W 16SW	Foliation Surface
CJ15-02	1	M2A	N60E 28NW	Not a significant surface (NSS)
CJ15-03	1	M1	Not oriented	
CJ15-04	1	M2B	Not oriented	
CJ15-05	1	M2B	Not oriented	
CJ15-06	2	M1	N30W 27SW	Foliation Surface, Collected by Marli Miller
CJ15-07	2	M1	N35W 35SW	Foliation Surface, Collected by Marli Miller
CJ-16 C101	1	Gneiss	N30W 47SW	NSS
CJ-16 C102	1	M1	N14E 49SW	NSS
CJ-16 C103	1	Gneiss	N55W 16NE	NSS
CJ-16 C104	1	M1	N69W 54NE	NSS
CJ-16 C105	1	M1	N11E 26NW	Foliation Surface
CJ-16 C106	1	Gneiss	N14W 82SW	NSS
CJ-16 C107	1	M2A	N5W 29SW	NSS
CJ-16 C108	1	Diabase	N24W 76SW	NSS
CJ-16 C109	1	M2B	N19W 16SW	Foliation Surface
CJ-16 C110	1	M2B	N25E 34NW	Foliation Surface
CJ-16 C111	1	M1	N80W 18NE	Foliation Surface
CJ-16 C112	1	M1	N32E 24NW	Foliation Surface
CJ-16 C201	2	M1	N25E 24NW	Foliation Surface
CJ-16 C202	2	Pegmatite	N30W 64SW	NSS
CJ-16 C203	2	M1	N23W 39SW	Foliation Surface
CJ-16 C204	2	Diabase	N70E 30NW	NSS
CJ-16 C205	2	Gneiss	N40W 43NE	NSS
CJ-16 C206	2	M2B	N11E 34SE	Foliation Surface
CJ-16 C207	2	Pegmatite	N43E 65NW	NSS
CJ-16 C208	2	M2B	N21E 45NW	Foliation Surface
CJ-16 C213	2	Breccia	N70E 39SE	Fault surface
CJ-16 C214	2	Breccia	No dip	NSS

## APPENDIX C

### THIN SECTIONS

Name	Canyon	Element	Plane Strike Orientation	Notes
CJ1501A	1	Gneiss	N55W	
CJ1502A	1	M2A	N58W	
CJ1502AP	1	M2A	N58W	
CJ1502BP	1	M2A	N32E	Perpendicular to CJ1502AP
CJ1506A	2	M1	N50W	
CJ1506AP	2	M1	N50W	
CJ1507A	2	M1	N80W	
CJ16C101	1	Gneiss	N60W	
CJ16C101P	1	Gneiss	N60W	
CJ16C102	1	M1	N60W	
CJ16C103A	1	Gneiss	N60W	
CJ16C103B	1	Gneiss	N30E	Perpendicular to CJ16C103A
CJ16C103AP	1	Gneiss	N60W	
CJ16C103BP	1	Gneiss	N30E	Perpendicular to CJ16C103AP
CJ16C104	1	M1	N60W	
CJ16C104AP	1	M1	N60W	
CJ16C105	1	M1	N60W	
CJ16C105P	1	M1	N60W	
CJ16C106	1	Gneiss	N13W	
CJ16C106P	1	Gneiss	N13W	
CJ16C107	1	M2A	N60W	
CJ16C108	1	Diabase	N60W	
CJ16C109A	1	M2B	N60W	
CJ16C109B	1	M2B	N20W	Cut along possible lineation
CJ16C110A	1	M2B	N0	
16C111AP	1	M1	N80W	
16C111BP	1	M1	N80W	
16C111CP	1	M1	N80W	
16C112AP	1	M1	N32E	

Name	Canyon	Element	Plane Strike Orientation	Notes
CJ16C201	2	M1	N60W	
16C201P	2	M1	N60W	
CJ16C202A	2	Pegmatite	N60W	
CJ16C202B	2	Pegmatite	N30E	Perpendicular to CJ16C202A
16C202AP	2	Pegmatite	N60W	
16C202BP	2	Pegmatite	N30E	Perpendicular to CJ16C202AP
CJ16C203	2	M1	N60W	
16C203P	2	M1	N60W	
16C203BP	2	M1	N30E	Perpendicular to 16C203P
CJ16C204	2	Diabase	N60W	
CJ16C205A	2	Gneiss	N25W	
CJ16C205B	2	Gneiss	N65E	Perpendicular to CJ16C205A
16C205AP	2	Gneiss	N25W	
16C205BP	2	Gneiss	N65E	Perpendicular to 16C205AP
CJ16C206A	2	M2B	N60W	
CJ16C206B	2	M2B	N60W	
16C206AP	2	M2B	N60W	
CJ16C207A	2	Pegmatite	N60W	
CJ16C207B	2	Pegmatite	N30E	Perpendicular to CJ16C207A
16C207AP	2	Pegmatite	N60W	
16C207BP	2	Pegmatite	N30E	Perpendicular to 16C207AP
CJ16C208A	2	M2B	N60W	
CJ16C208B	2	M2B	N11W	Cut along possible lineation
16C208AP	2	M2B	N60W	
16C208BP	2	M2B	N11W	
16C213AP	2	Breccia	N20W	Cut perpendicular to fault surface
16C214AP	2	Breccia	N20W	Cut perpendicular to fault surface

## REFERENCES CITED

- Anderson, E.R., 1971, Thin skin distension in tertiary rocks of southeastern Nevada: Geological Society of America Bulletin, v. 82, p. 43–58, doi: 10.1130/0016-7606(1971)82[43:TSDITR]2.0.CO;2.
- Armstrong, R.L., 1982, Cordilleran Metamorphic Core Complexes - From Arizona to Southern Canada: Annual Review of Earth and Planetary Sciences, v. 10, p. 129–154, doi: 10.1017/CBO9781107415324.004.
- Atkinson, B.K., 1987, Introduction to fracture mechanics and its geophysical applications, *in* Atkinson, B. K. (ed.), Fracture Mechanics of Rock: Academic Press, London, p. 1-26.
- Bestmann, M., Kunze, K., and Matthews, A., 2000, Evolution of a calcite marble shear zone complex on Thassos Island, Greece: Microstructural and textural fabrics and their kinematic significance: Journal of Structural Geology, v. 22, p. 1789–1807, doi: 10.1016/S0191-8141(00)00112-7.
- Bowen, N.L., 1940, Progressive Metamorphism of Siliceous Limestone and Dolomite: The Journal of Geology, v. 48, p. 225–274.
- Burchfiel, B.C., and Stewart, J.H., 1966, “pull-apart” origin of the central segment of Death Valley, California: Geological Society of America Bulletin, v. 77, p. 439–442, doi: 10.1130/0016-7606(1966)77[439:POOTCS]2.0.CO;2.
- Burkhard, M., 1993, Calcite twins, their geometry, appearance and significance as stress-strain markers and indicators of tectonic regime: a review: Journal of Structural Geology, v. 15, p. 351–368, doi: 10.1016/0191-8141(93)90132-T.
- Butler, P.R., Troxel, B.W., and Verosub, K.L., 1988, Late Cenozoic history and styles of deformation along the southern Death Valley fault zone, California: Geological Society of America Bulletin, v. 100, p. 402–410, doi: 10.1130/0016-7606(1988)100<0402:LCHASO>2.3.CO;2.
- Cemen, I., Tekeli, O., Seyitoglu, G., and Isik, V., 2005, Are turtleback fault surfaces common structural elements of highly extended terranes? Earth-Science Reviews, v. 73, p. 139–148, doi: 10.1016/j.earscirev.2005.07.001.
- Cowan, D.S., Cladouhos, T.T., and Morgan, J.K., 2003, Structural geology and kinematic history of rocks formed along low - angle normal faults, Death Valley, California: Geological Society of America Bulletin, v. 115, p. 1230–1248, doi: 10.1130/B25245.1.

- Creveling, J.R., Bergmann, K.D., and Grotzinger, J.P., 2016, Cap carbonate platform facies model, Noonday Formation, SE California: Geological Society of America Bulletin, v. 128, p. 1249–1269, doi: 10.1130/B31442.1.
- Curry, D. H., 1938, “Turtleback” fault surfaces in Death Valley, California: Abstract, Geological Society of America Bulletin, v. 49, p. 1875.
- Curry, D.H., 1954, Turtlebacks in the Central Black Mountains, Death Valley, California in Geology of Southern California: California Division of Mines and Geology, Bulletin 170, v. 2, p.53-59.
- Davis, G. a, and Lister, G.S., 1988, Detachment faulting in continental extension; Perspectives from the Southwestern U.S. Cordillera: Geological Society of America Special Papers, v. 218, p. 133–160, doi: 10.1130/SPE218-p133.
- De Bresser, J.H.P., Evans, B., and Renner, J., 2002, On estimating the strength of calcite rocks under natural conditions (S. De Meer, M. R. Drury, J. H. P. De Bresser, & G. M. Pennock, Eds.): Geological Society, London, Special Publications, v. 200, p. 309–329, doi: 10.1144/GSL.SP.2001.200.01.18.
- DiCiccio, T.J., and Efron, B., 1996, Bootstrap Confidence Intervals: Statistical Science, v. 11, p. 189–228, doi: 10.1007/s10869-007-9037-x.
- Dokka, R.K., and Ross, T.M., 1995, Collapse of Southwestern North-America and the Evolution of Early Miocene Detachment Faults, Metamorphic Core Complexes, the Sierra-Nevada Orocline, and the San-Andreas Fault System: Geology, v. 23, p. 1075–1078.
- Drewes, H., 1959, Turtleback Faults of Death Valley, California: A Reinterpretation: Geological Society of America Bulletin, v. 70, no. 12, p. 1497-1508.
- Eggert, R.G., and Kerrick, D.M., 1981, Metamorphic equilibria in the siliceous dolomite system: 6 kbar experimental data and geologic implications: Geochimica et Cosmochimica Acta, v. 45, p. 1039–1049, doi: 10.1016/0016-7037(81)90130-7.
- Erslev, E.A., 1988, Normalized center-to-center strain analysis of packed aggregates: Journal of Structural Geology, v. 10, p. 201–209, doi: 10.1016/0191-8141(88)90117-4.
- Erslev, E.A., and Ge, H., 1990, Least-squares center-to-center and mean object ellipse fabric analysis: Journal of Structural Geology, v. 12, p. 1047–1059, doi: 10.1016/0191-8141(90)90100-D.
- Faulds, J.E., Henry, C.D., and Hinz, N.H., 2005, Kinematics of the northern Walker Lane: An incipient transform fault along the Pacific-North American plate boundary: Geology, v. 33, p. 505–508, doi: 10.1130/G21274.1.

- Ferrill, D.A., 1991, Calcite twin widths and intensities as metamorphic indicators in natural low-temperature deformation of limestone: *Journal of Structural Geology*, v. 13, p. 667–675, doi: 10.1016/0191-8141(91)90029-I.
- Ferrill, D.A., 1998, Critical re-evaluation of differential stress estimates from calcite twins in coarse-grained limestone: *Tectonophysics*, v. 285, p. 77–86, doi: 10.1016/S0040-1951(97)00190-X.
- Ferrill, D.A., Morris, A.P., Evans, M.A., Burkhard, M., Groshong, R.H., and Onasch, C.M., 2004, Calcite twin morphology: A low-temperature deformation geothermometer: *Journal of Structural Geology*, v. 26, p. 1521–1529, doi: 10.1016/j.jsg.2003.11.028.
- Flesch, L., and Bendick, R., 2012, The relationship between surface kinematics and deformation of the whole lithosphere: *Geology*, v. 40, p. 711–714, doi: 10.1130/G33269.1.
- Fry, N., 1979, Random point distributions and strain measurement in rocks: *Tectonophysics*, v. 60, p. 89–105, doi: 10.1016/0040-1951(79)90135-5.
- Gordon, T.M., and Greenwood, H.J., 1970, The Reaction: Dolomite + Quartz + Water = Talc + Calcite + Carbon Dioxide: *American Journal of Science*, v. 268, p. 225–242.
- Groshong Jr., R.H., 1974, Experimental Test of Least-Squares Strain Gage Calculation Using Twinned Calcite: *Geological Society of America Bulletin*, v. 85, p. 1855–1864.
- Groshong Jr., R.H., 1988, Low Temperature Deformation Mechanisms and their Interpretation: *Geological Society of America Bulletin*, v. 100, p. 1329–1360.
- Groshong Jr., R.H., 1972, Strain Calculated from Twinning in Calcite: *Geological Society of America Bulletin*, v. 83, p. 2025–2038.
- Groshong Jr., R.H., Teufel, L.W., and Gasteiger, C., 1984, Precision and accuracy of the calcite strain-gage technique: *Geological Society of America Bulletin*, v. 95, p. 357, doi: 10.1130/0016-7606(1984)95<357:PAAOTC>2.0.CO;2.
- Hamilton, W.B., 1988, Detachment faulting in the Death Valley region: California and Nevada: *Geologic and Hydrologic Investigations, Yucca Mountain, Nevada*, p. 51–85.
- Hamilton, W., and Myers, W.B., 1966, Cenozoic Tectonics of the Western United States: *Reviews of Geophysics*, v. 4.

- Hayman, N.W., 2006, Shallow crustal fault rocks from the Black Mountain detachments, Death Valley, CA: *Journal of Structural Geology*, v. 28, p. 1767–1784, doi: 10.1016/j.jsg.2006.06.017.
- Hayman, N.W., Knott, J.R., Cowan, D.S., Nemser, E., and Sarna-Wojcicki, A.M., 2003, Quaternary low-angle slip on detachment faults in Death Valley, California: *Geology*, v. 31, p. 343–346, doi: 10.1130/0091-7613(2003)031<0343:QLASOD>2.0.CO;2.
- Hill, M.L., and Troxel, B.W., 1966, Tectonics of Death Valley Region California: *Geological Society of America Bulletin*, v. 77, p. 435–438, doi: 10.1130/0016-7606(1966)77[435:todvrc]2.0.co;2.
- Hirth, G., and Tullis, J., 1992, Dislocation creep regimes in quartz aggregates: *Journal of Structural Geology*, v. 14, p. 145–159, doi: 10.1016/0191-8141(92)90053-Y.
- Holm, D.K., and Dokka, R.K., 1993, Interpretation and tectonic implications of cooling histories: An example from the Black Mountains, Death Valley extended terrane, California: *Earth and Planetary Science Letters*, v. 116, p. 63–80, doi: 10.1016/0012-821X(93)90045-B.
- Holm, D.K., Snow, J.K., and Lux, D.R., 1992, Thermal and barometric constraints on the intrusive and unroofing history of the Black Mountains: Implications for timing, initial dip, and kinematics of detachment faulting in the Death Valley Region, California: *Tectonics*, v. 11, p. 507–522, doi: 10.1029/92TC00211.
- Holm, D.K., Fleck, R.J., and Lux, D.R., 1994, The Death Valley Turtlebacks Reinterpreted as Miocene-Pliocene Folds of a Major Detachment Surface: *The Journal of Geology*, v. 102, p. 718–727.
- Holm, D.K., and Wernicke, B., 1990, Black Mountains crustal section, Death Valley extended terrain, California: *Geology*, v. 18, p. 520–523, doi: 10.1130/0091-7613(1990)018<0520:BMCSDV>2.3.CO;2.
- Hunt, C.B., and Mabey, D.R., 1966, Stratigraphy and Structure Death Valley, California: *USGS Professional Paper*, v. 494–A, p. 156.
- I. Wright, S., M. Nowell, M., and P. Field, D., 2011, A Review of Strain Analysis Using Electron Backscatter Diffraction: *Microscopy and Microanalysis*, v. 17, p. 316–329.
- Keener, C., Serpa, L., and Pavlis, T.L., 1993, Faulting at Mormon Point, Death Valley, California: a low-angle normal fault cut by high-angle faults: *Geology*, v. 21, p. 327–330, doi: 10.1130/0091-7613(1993)021<0327:FAMPDV>2.3.CO;2.



- Kennedy, L.A., and White, J.C., 2001, Low-temperature recrystallization in calcite: Mechanisms and consequences: *Geology*, v. 29, p. 1027–1030, doi: 10.1130/0091-7613(2001)029<1027:LTRICM>2.0.CO.
- Knott, J., Sarnawojcicki, A., Machette, M., and Klinger, R., 2005, Upper Neogene stratigraphy and tectonics of Death Valley — a review: *Earth-Science Reviews*, v. 73, p. 245–270, doi: 10.1016/j.earscirev.2005.07.004.
- Kushnir, A.R.L., Kennedy, L.A., Misra, S., Benson, P., and White, J.C., 2015, The mechanical and microstructural behaviour of calcite-dolomite composites: An experimental investigation: *Journal of Structural Geology*, v. 70, p. 200–216, doi: 10.1016/j.jsg.2014.12.006.
- Lacombe, O., 2010, Calcite twins, a tool for tectonic studies in thrust belts and stable orogenic forelands: *Oil & Gas Science and Technology – Revue d’IFP Energies nouvelles*, v. 65, p. 809–838, doi: 10.2516/ogst/2009088.
- Lister, G.S., and Snoke, a. W., 1984, S-C Mylonites: *Journal of Structural Geology*, v. 6, p. 617–638, doi: 10.1016/0191-8141(84)90001-4.
- Lister, G.S., and Davis, G. a, 1989, The origin of metamorphic core complexes and detachment faults formed during Tertiary continental extension in the northern Colorado River region, U.S.A.: *Journal of Structural Geology*, v. 11, p. 65–94, doi: 10.1016/0191-8141(89)90036-9.
- Mancktelow, N.S., and Pavlis, T.L., 1994, Fold-fault relationships in low-angle detachment systems: *Tectonics*, v. 13, p. 668–685, doi: 10.1029/93TC03489.
- Meere, P.A., and Mulchrone, K.F., 2003, The effect of sample size on geological strain estimation from passively deformed clastic sedimentary rocks: *Journal of Structural Geology*, v. 25, p. 1587–1595, doi: 10.1016/S0191-8141(03)00007-5.
- Miller, M., 1991, High-angle origin of the currently low-angle Badwater Turtleback fault , Death Valley, California: *Geology*, p. 372–375, doi: 10.1130/0091-7613(1991)019<0372:HAOTC>2.3.CO;2.
- Miller, M., 1992, Brittle Faulting Induced By Ductile Deformation of a Rheologically Stratified Rock Sequence, Badwater Turtleback, Death-Valley, California: *Geological Society of America Bulletin*, v. 104, p. 1376–1385, doi: 10.1130/0016-7606(1992)104<1376:bfibdd>2.3.co;2.
- Miller, M., 1996, Ductility in fault gouge from a normal fault system, Death Valley, California: A mechanism for fault-zone strengthening and relevance to paleoseismicity: *Geology*, v. 24, p. 603–606, doi: 10.1130/0091-7613(1996)024<0603:DIFGFA>2.3.CO;2.

- Miller, M., 2003, Basement-involved thrust faulting in a thin-skinned fold-and-thrust belt, Death Valley, California, USA: *Geology*, v. 31, p. 31–34, doi: 10.1130/0091-7613(2003)031<0031:BITFIA>2.0.CO;2.
- Miller, M., 2005, Geological landscapes of the Death Valley region☆: *Earth-Science Reviews*, v. 73, p. 17–30, doi: 10.1016/j.earscirev.2005.07.010.
- Miller, M., and Friedman, R.M., 1999, Early Tertiary magmatism and probable Mesozoic fabrics in the Black Mountains, Death Valley, California: *Geology*, v. 27, p. 19–22, doi: 10.1130/0091-7613(1999)027<0019:ETMAPM>2.3.CO;2.
- Miller, M., and Pavlis, T., 2005, The Black Mountains turtlebacks: Rosetta stones of Death Valley tectonics: *Earth-Science Reviews*, v. 73, p. 115–138, doi: 10.1016/j.earscirev.2005.04.007.
- Miller, M., and Prave, A.R., 2002, Rolling hinge or fixed basin?: A test of continental extensional models in Death Valley, California, United States: *Geology*, v. 30, p. 847–850, doi: 10.1130/0091-7613(2002)030<0847:RHOFA>2.0.CO;2.
- Mulchrone, K.F., 2003, Application of Delaunay triangulation to the nearest neighbour method of strain analysis: *Journal of Structural Geology*, v. 25, p. 689–702, doi: 10.1016/S0191-8141(02)00067-6.
- Mulchrone, K.F., McCarthy, D.J., and Meere, P.A., 2013, Computers & Geosciences Mathematica code for image analysis, semi-automatic parameter extraction and strain analysis: *Computers and Geosciences*, v. 61, p. 64–70, doi: 10.1016/j.cageo.2013.08.001.
- Mulchrone, K.F., O’Sullivan, F., and Meere, P.A., 2002, Finite strain estimation using the mean radial length of elliptical objects with bootstrap confidence intervals: *Journal of Structural Geology*, v. 25, p. 529–539, doi: 10.1016/S0191-8141(02)00049-4.
- Noble, L.F., 1934, Rock formations of Death Valley, California: *Science*, v. 80, no. 2069, p. 173-178.
- Noble, L.F., 1941, Structural Features of the Virgin Spring Area, Death Valley, California: *Bulletin of the Geologic Society of America*, v. 52, p. 941-1000.
- Noble, L.F., and Wright, L.A., 1954, Geology of the Central and Southern Death Valley Region, California *in* *Geology of Southern California*: California Division of Mines and Geology, Bulletin 170, v. 2, p. 143-160.
- Norton, I., 2011, Two-stage formation of Death Valley: *Geosphere*, v. 7, p. 171–182, doi: 10.1130/GES00588.1.

- Prior, D.J., Boyle, A. P., Brenker, F., Cheadle, M.C., Day, A., Lopez, G., Peruzzo, L., Potts, G.J., Reddy, S., Spiess, R., Timms, N.E., Trimby, P., Wheeler, J., Zetterstrom, L., 1999, The application of electron backscatter diffraction and orientation contrast imaging in the SEM to textural problems in rocks: *American Mineralogist*, v. 84, p. 1741–1759, doi: 10.2138/am-1999-11-1204.
- Rogowitz, A., Grasemann, B., Huet, B., and Habler, G., 2014, Strain rate dependent calcite microfabric evolution - An experiment carried out by nature: *Journal of Structural Geology*, v. 69, p. 1–17, doi: 10.1016/j.jsg.2014.08.004.
- Rutter, E.H., 1972, The influence of interstitial water on the rheological behaviour of calcite rocks: *Tectonophysics*, v. 14, p. 13–33, doi: 10.1016/0040-1951(72)90003-0.
- Rutter, E.H., 1974, The influence of temperature, strain rate and interstitial water in the experimental deformation of calcite rocks: *Tectonophysics*, v. 22, p. 311–334, doi: 10.1016/0040-1951(74)90089-4.
- Rybacki, E., Evans, B., Janssen, C., Wirth, R., and Dresen, G., 2013, Influence of stress, temperature, and strain on calcite twins constrained by deformation experiments: *Tectonophysics*, v. 601, p. 20–36, doi: 10.1016/j.tecto.2013.04.021.
- Rybacki, E., Janssen, C., Wirth, R., Chen, K., Wenk, H.R., Stromeyer, D., and Dresen, G., 2011, Low-temperature deformation in calcite veins of SAFOD core samples (San Andreas Fault) - Microstructural analysis and implications for fault rheology: *Tectonophysics*, v. 509, p. 107–119, doi: 10.1016/j.tecto.2011.05.014.
- Schmandt, B., and Humphreys, E., 2011, Seismically imaged relict slab from the 55 Ma Siletzia accretion to the northwest United States: *Geology*, v. 39, p. 175–178, doi: 10.1130/G31558.1.
- Schmid, S.M., Panozzo, R., and Bauer, S., 1987, Simple shear experiments on calcite rocks: rheology and microfabric: *Journal of Structural Geology*, v. 9, p. 747–778, doi: 10.1016/0191-8141(87)90157-X.
- Sears, D.H., 1953, Origin of the Amargosa Chaos, Virgin Spring Area, Death Valley, California: *The Journal of Geology*, v. 61, no. 2, p. 182-186.
- Serpa, L., and Pavlis, T.L., 1996, Three-dimensional model of the late Cenozoic history of the Death Valley region, southeastern California: *Tectonics*, v. 15, p. 1113–1128, doi: 10.1029/96tc01633.
- Snow, J.K., and Wernicke, B.P., 2000, Cenozoic tectonism in the central basin and range: Magnitude, rate, and distribution of upper crustal strain: *American Journal of Science*, v. 300, p. 659–719, doi: 10.2475/ajs.300.9.659.

- Stewart, J.H., 1983, Extensional tectonics in the Death Valley area, California: Transport of the Panamint Range structural block 80 km northwestward: *Geology*, v. 11, p. 153, doi: 10.1130/0091-7613(1983)11<153.
- Stipp, M., Stünitz, H., Heilbronner, R., and Schmid, S.M., 2002, The eastern Tonale fault zone: A “natural laboratory” for crystal plastic deformation of quartz over a temperature range from 250 to 700 C: *Journal of Structural Geology*, v. 24, p. 1861–1884, doi: 10.1016/S0191-8141(02)00035-4.
- Topping, D.J., 1993, Paleogeographic reconstruction of the Death Valley extended region: evidence from Miocene large rock-avalanche deposits in the Amargosa Chaos Basin, California: *Geological Society of America Bulletin*, v. 105, p. 1190–1213, doi: 10.1130/0016-7606(1993)105<1190:PROTDV>2.3.CO;2.
- Van der Pluijm, B. A., 1991, Marble mylonites in the Bancroft shear zone, Ontario, Canada: microstructures and deformation mechanisms: *Journal of Structural Geology*, v. 13, p. 1125–1135.
- Vollmer, F., 2015, Orient 3: a new integrated software program for orientation data analysis, kinematic analysis, spherical projections, and Schmidt plots.: *Geological Society of America Abstracts with Programs*, v. 47, p. 49.
- Waldron, J.W.F., and Wallace, K.D., 2007, Objective fitting of ellipses in the centre-to-centre (Fry) method of strain analysis: *Journal of Structural Geology*, v. 29, p. 1430–1444, doi: 10.1016/j.jsg.2007.06.005.
- Weeks, W.F., 1956, A Thermochemical Study of Equilibrium Relations during Metamorphism of Siliceous Carbonate Rocks: *The Journal of Geology*, v. 64, p. 245–270.
- Wenk, H.R., Takeshita, T., Bechler, E., Erskine, B.G., and Matthies, S., 1987, Pure shear and simple shear calcite textures. Comparison of experimental, theoretical and natural data: *Journal of Structural Geology*, v. 9, p. 731–745, doi: 10.1016/0191-8141(87)90156-8.
- Wernicke, B., Axen, G., and Snow, J., 1988, Basin and Range extensional tectonics at the latitude of Las Vegas, Nevada: *Geological Society of ...*, v. 100, p. 1738–1757.
- Wernicke, B., Davis, J.L., Niemi, N.A., Luffi, P., and Bisnath, S., 2008, Active megadetachment beneath the western United States: *Journal of Geophysical Research: Solid Earth*, v. 113, p. 1–26, doi: 10.1029/2007JB005375.
- Whitney, D.L., Hirschmann, M., and Miller, M., 1993, Zincian ilmenite - eandrewsite from a pelitic schist, Death Valley, California, and the paragenesis of (Zn,Fe)TiO<sub>3</sub> solid solution in metamorphic rocks: *Canadian Mineralogist*, v. 31, p. 425–436.

Wright, L., 1976, Late Cenozoic fault patterns and stress fields in the Great Basin and westward displacement of the Sierra Nevada block: *Geology*, v. 4, p. 489–494, doi: 10.1130/0091-7613(1976)4<489:LCFPAS>2.0.CO;2.

Wright, L.A., Green, R., Cemen, I., Johnson, R., and Prave, A., 1999, Tectonostratigraphic development of the Miocene-Pliocene Furnace Creek Basin, Death Valley, California, in Wright, L.A., and Troxel, B.W. eds., *Tertiary basins in the Death Valley region, California*. Geological Society of America Special Paper 333, p. 87-114.

Wright, L.A., Otton, J.K., and Troxel, B.W., 1974, Turtleback Surfaces of Death Valley Viewed as Phenomena of Extensional Tectonics: *Geology*, v. 2, p. 53–54, doi: 10.1130/0091-7613(1974)2<53:TSODVV>2.0.CO;2.

Wright, L.A., Thompson, R.A., Troxel, B.W., Pavlis, T.L., DeWitt, D.H., Otton, J.K., Ellis, P.G., Miller, M.B., and Serpa, L.F., 1991, Cenozoic magmatic and tectonic evolution of the east-central Death Valley region, California, *in* Walawender, M.J., and Hannan, B.B., eds., *Geologic excursions in southern California and Mexico*: San Diego, Department of Geological Sciences, San Diego State University, p. 93-127.

Wright, L.A., Troxel, B.W., Williams, E.G., Roberts, M.T., and Diehl, P.E., 1976, Precambrian sedimentary environments of the Death Valley region, eastern California: California Division of Mines and Geology Special Report 106: *Geologic Features of Death Valley, California*, p. 27–36.